Applied Energy 404 (2026) 127140

Contents lists available at ScienceDirect

Applied Energy

journal homepage: www.elsevier.com/locate/apen

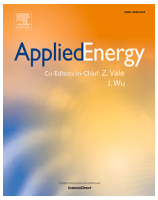

Power system planning under deep uncertainty: Integrating tidal energy for net-zero Northern Ireland

Vahid Sabzpoosh Saravi [a,*], Xueqin Liu [a,*], Carwyn Frost [b]

[a] School of Electronics, Electrical Engineering and Computer Science, Queen's University Belfast, Belfast, BT9 5AH, UK
[b] School of Natural and Built Environment, Queen's University Belfast, Belfast, BT9 5AH, UK

HIGHLIGHTS

- A techno-economic optimization model that integrates tidal energy into power system is proposed to achieve Northern Ireland's net-zero emissions targets by 2030.
- Energy storage solutions are explored to enhance the contribution of tidal energy to grid stability and reliability in renewable energy systems.
- The model incorporates dispatch-down cost and CO_2 emission penalty scenarios to analyze its role in reducing dispatch down and carbon emissions.
- The potential of offshore wind and tidal energy sources as optimal techno-economic solutions is compared for future energy systems.
- The study assesses the relatively underexplored advantages of tidal energy in facilitating its integration at the grid scale.

ARTICLE INFO

Keywords:
Tidal energy
Net-zero emissions
Battery and hydrogen energy storage
Heating electrification
Techno-economic analysis

ABSTRACT

Achieving high renewable penetration is often hindered by resource variability, renewable curtailment, and deep uncertainties in long-term decarbonization planning. In coastal and islanded power systems with significant tidal potential, predictable marine resources such as tidal power can offer a valuable solution, enhancing system flexibility, reducing curtailment, and supporting progress towards net-zero objectives. In Northern Ireland, however, tidal energy remains underutilized, and limited operational flexibility continues to pose challenges for integrating large shares of renewables. To address these challenges, this paper proposes a robust multi-period power system planning framework that integrates tidal energy and energy storage using an Information Gap Decision Theory–Flexible Revision Multi-period Two-stage Stochastic Planning (IG-FRM-TSP) model. The framework explicitly accounts for uncertainties in demand growth, technology costs, and CO_2 pricing, while optimizing the coordinated deployment of tidal, offshore wind, and hydrogen-battery storage. A novel Dispatch Down Reduction Index (DDRI) is introduced to quantify and reduce renewable curtailment, improving system efficiency and flexibility. Scenario analyses show that strategic co-deployment of tidal energy with offshore wind and storage can reduce curtailment to below 2 %, while achieving up to 80 % CO_2 emissions reduction compared to business-as-usual scenarios, all while maintaining grid reliability. The results highlight that tidal predictability, combined with responsive storage and supportive policy incentives, plays a critical role in enabling cost-effective decarbonization pathways for islanded and coastal power systems. The proposed methodology offers a replicable approach for similar regions worldwide, emphasizing that operational coordination and market design—beyond capacity expansion—are essential to achieving net-zero goals.

1. Introduction

As global efforts to combat climate change intensify, transitioning to renewable energy sources has become imperative. Northern Ireland, endowed with substantial marine resources, is uniquely positioned to harness offshore renewables, particularly tidal energy and offshore wind, to enhance energy security and contribute meaningfully to national net-zero targets. Despite significant advances in offshore wind deployment, tidal energy remains underexploited. Comprehensive planning frameworks that integrate tidal power's high predictability and complementary role with intermittent renewables, alongside evolving

* Corresponding authors.
Email addresses: vahid.sabzpoosh@yahoo.com (V. Sabzpoosh Saravi), x.liu@qub.ac.uk (X. Liu).

https://doi.org/10.1016/j.apenergy.2025.127140
Received 2 October 2025; Received in revised form 14 November 2025; Accepted 22 November 2025
Available online 3 December 2025

Nomenclature

Indices

$\mathcal{T}, t$	Indices of planning periods and time
g, st	Indices of generation and storage units
i, j	Indices of electricity network buses
s	Index of scenario
t_{rev}	Index of revision time

Parameters

α^*	The robustness function from IGDT
β	Deviation parameter for uncertainty
λ	Weighting factor for the regret term
μ	Weighting factor for the robustness term
$\overline{P}^{D,EL}$	Electrolyzer capacity
$\overline{P_{st}}$	Rated power of storage st
$\underline{P}_g, \overline{P}_g$	Minimum and maximum active power generation
$\underline{P}_{ij}, \overline{P}_{ij}$	Minimum and maximum power flow limits
$\underline{Q}_g, \overline{Q}_g$	Minimum and maximum reactive power generation
$\underline{SoC}_{st}, \overline{SoC}_{st}$	Minimum and maximum state of charge
$\underline{V}_i, \overline{V}_i$	Minimum and maximum voltage limits
C_{th}	Maximum acceptable level for total cost
COP	Heat pump coefficient of performance
δ_1, δ_2	Multiplicative factors applied to the CO_2 cost
$\eta_{st}^{ch}, \eta_{st}^{dis}$	Charging and discharging efficiency of storage st
η^{EL}, η^{FC}	Electrolyzer and fuel cell efficiency
η^{HP}	Heat pump efficiency
ξ^{obs}	Observed uncertainty parameter
ξ_s	Realized uncertainty parameter for scenarios s
B_{ii}^y, G_{ii}^y	Self susceptance and conductance
B_{ij}^y, G_{ij}^y	Mutual susceptance and conductance
B_t	Available budget at time t
cap_{low}, cap_{high}	Emission thresholds
c_s^{DD}	Dispatch down per unit cost in scenario s
c^{elec}, c^{gas}	Electricity and gas costs
C_g^{Inv}, C_{st}^{Inv}	Investment cost for generation and storage units
C_s^{Ope}	The operational costs in scenario s
C^{total}	The objective function value
$C_s^{CO_2}$	CO_2 emission cost in scenario s
$e_t^{CO_2}$	CO_2 emissions at time t
LHV_{H2}	Lower heating value of hydrogen
OC^F	Fixed operational cost
OC^V	Variable operational cost
$P_{i,t}^D, Q_{i,t}^D$	Active and reactive power demand at bus i
p_s	Probability of scenario s
sub_t^{Tidal}	The subsidy applied to the tidal investment

Sets

S	Set of all possible scenarios
Ω^{Co}	Set of interconnectors
Ω^g	Set of generation units
Ω^n	Set of power network buses
Ω^{Re}	Set of renewable generations
Ω^{st}	Set of storage units
Ω^{Tidal}	Set of tidal energy resources
X_t	Set of feasible investment decisions
$Y_{s,t}$	Set of feasible operational decisions

Variables

$P_{ij,t}, Q_{ij,t}$	Active and reactive power flow between buses i and j
$DD_{g,t}$	Dispatch down of renewable source g at time t
$f_t^{D,FC}$	Fuel cell hydrogen consumption
$f^{EL}t$	Electrolyzer hydrogen generation
$f_{st,t}^{H2,ch}, f_{st,t}^{H2,dis}$	Hydrogen storage charge and discharge rate
$P_{E,i,t}^{D,EL}$	Electrolyzer power consumption at bus i
$P_{i,t}^{ex}$	Interconnectors power exchange
$P_{E,i,t}^{FC}$	Fuel cell power generation at bus i
$P_{Th,k,t}^{HP}$	Heat pump thermal output at node k
$P_{Th,k,t}^{HP}, P_{E,i,t}^{D,HP}$	Heat pump thermal generation and power consumption at bus i
$P_{i,g,t}, Q_{i,g,t}$	Active and reactive power generation at bus i
$P_{i,st,t}^{ch}, P_{i,st,t}^{dis}$	Charge and discharge power of storage st at bus i
$P_{i,t}^{inj}, P_{i,t}^{inj}$	Active and reactive power injection at bus i
$SoC_{st,t}$	State of charge of storage st at time t
$V_{i,t}, \theta_{i,t}$	Voltage magnitude and angle at bus i
$x_{st,t}^{ch}$	Binary variable for storage charging status
$x_t^{initial}$	Initial decision for investment
$x_{g,t}$	Binary variable for generation units investment
$x_{st,t}$	Binary variable for storage units investment decision

storage technologies such as hydrogen energy storage, are critically needed.

Northern Ireland has a statutory obligation to ensure that at least 80 % of its electricity consumption comes from renewable sources by 2030 [1]. While wind power will remain the dominant renewable resource, this target will significantly intensify operational challenges already evident today, including high levels of dispatch-down, network congestion, and limits on non-synchronous generation required to maintain system stability. Without the integration of complementary resources and new planning approaches, these challenges are expected to grow, risking both economic efficiency and security of supply. This forms a central motivation for the present study, which investigates the role of tidal energy within an integrated operational planning framework to enhance renewable utilization and system robustness.

Current long-term power system planning models often inadequately address the combined integration of tidal energy and hydrogen storage, especially under deep uncertainties including fluctuating demand, technology costs, and regulatory environments. Furthermore, many models lack the flexibility to dynamically revise strategic plans over multiple periods, limiting adaptability amid the rapidly evolving energy landscape. These limitations reveal a clear research gap in developing robust, scalable frameworks that guide net-zero-aligned power system expansion incorporating tidal energy and advanced storage solutions.

To bridge this gap, this paper proposes a novel Information Gap Decision Theory (IGDT) and Flexible Revision Multi-period Two-stage Stochastic Planning (IG-FRM-TSP) methodology. By integrating IGDT's robustness to deep uncertainty with a flexible multi-period revision structure, IG-FRM-TSP enables strategic plan adjustments across multiple horizons while capturing interactions among tidal generation, hydrogen storage, and the broader power system. This methodology extends beyond prior IGDT applications focused mainly on short-term operational decisions or isolated subsystems, offering a comprehensive long-term planning tool for resilient, low-carbon energy systems.

Northern Ireland's marine environment offers a unique opportunity to integrate tidal energy with offshore wind and heating electrification, creating a diversified and stable energy system. Offshore wind has rapidly expanded over the past decade, solidifying its role in the energy transition [2]. In contrast, tidal energy's high predictability and consistent capacity factors present a valuable yet underutilized resource to complement variable wind and solar generation [3]. This predictability

enhances grid stability and reduces variability when tidal power is combined with other renewables, strengthening supply reliability [4,5].

Tidal energy harnesses the gravitational forces of the moon and sun, producing renewable power with regular, forecastable cycles. Advances in tidal stream and tidal range converters have improved capture efficiency and operational performance [6], expanding tidal energy's potential in coastal renewable portfolios. Though currently costlier than mature renewables, innovation and economies of scale are expected to lower costs, improving feasibility for large-scale integration [7,8]. These developments, coupled with supportive policies, reinforce tidal energy's emerging role in future energy systems. Recent evidence reinforces that tidal energy can become an economically viable option under large-scale deployment supported by targeted policy and innovation measures. According to [9], although tidal stream energy currently entails high upfront costs, systematic cost reductions are achievable through learning-by-doing and technological innovation, provided that continued deployment support—such as market subsidies and research funding—is maintained. Their analysis quantified that sustaining learning rates of 12.5 %–15 % could substantially lower the levelized cost of tidal electricity, with economic competitiveness expected once deployment reaches the multi-hundred-megawatt scale. Building on these insights, the present study extends this perspective by applying a real regional case in Northern Ireland to assess long-term economic feasibility under future large-scale deployment scenarios.

The complementary nature of tidal energy relative to intermittent renewables has attracted growing research interest. Studies demonstrate that co-locating tidal stream power with offshore wind farms can enhance grid stability and balance supply–demand fluctuations [10]. Despite over 30 GW of untapped marine energy potential in the UK [11], tidal energy remains underutilized in Northern Ireland. Harnessing these marine resources offers opportunities for regional economic growth, energy resilience, and technological innovation.

Northern Ireland's proximity of tidal and offshore wind resources near existing transmission infrastructure offers cost-effective integration pathways. Nevertheless, interactions between tidal energy, other renewables, and their aggregated operational impacts require deeper investigation. Addressing these interactions and their economic implications constitutes a key contribution of this study.

Electrification of heating is an essential pillar of end-use decarbonization. As fossil-fuel heating is phased out, coupling renewables with electrified heating is vital to emission reduction efforts [12]. Integrating tidal energy with heating electrification necessitates a thorough understanding of storage solutions to manage variability and ensure reliability.

Prior research predominantly examines heat electrification in wind-powered systems using heat pumps and thermal storage [13], while studies on tidal integration remain sparse. Tidal energy's predictable generation profile offers distinct grid management and curtailment reduction potential compared to wind. For example, the European Marine Energy Centre (EMEC) demonstrated that coupling tidal power with flow batteries enables continuous green hydrogen production, showcasing innovative storage and grid balancing applications [14]. These examples underscore the need for integrated planning models that capture tidal's synergy with other renewables and storage technologies to minimize curtailment and maximize system flexibility.

Energy storage systems (ESS) play a critical role in mitigating renewable intermittency, enhancing grid stability and dispatchability [15]. Recent studies emphasize the assessment of diverse ESS technologies—including batteries, pumped hydro, and emerging hydrogen storage—especially in offshore renewable contexts [15,16], which is vital for optimizing renewable integration and ensuring grid reliability.

Specifically, Ref. [17] highlights ESS's importance in improving tidal energy dispatchability and supply reliability by smoothing the intermittency typical of solar and wind. However, economic analyses of storage options paired with tidal remain limited, indicating a significant gap in optimizing cost-effective storage solutions [17,18].

Reviews such as [19] focus primarily on renewable integration and storage for wind and solar in Europe, providing limited insight into tidal's unique characteristics and challenges. Related work [20] analyses wind farm storage, finding economic benefits from price arbitrage and mixed curtailment effects, yet these findings do not extend to tidal systems. This highlights the need for ESS strategies tailored specifically to tidal power dynamics.

The offshore ESS literature [21] largely addresses wind farm applications, discussing batteries, supercapacitors, and flywheels. Tidal energy integration challenges remain underrepresented, revealing another research gap.

A major operational challenge in Northern Ireland is "dispatch down," where renewable generation is curtailed below available capacity due to grid constraints or system stability requirements [22]. Transmission limits and security concerns exacerbate this issue. To address it, this study introduces a Dispatch Down Reduction Index (DDRI) that quantifies renewable curtailment, including tidal energy, providing a metric to minimize dispatch down. Incorporating DDRI incentivizes maximizing clean energy utilization, improving overall efficiency and reliability.

Economic evaluation is fundamental for assessing renewable project feasibility. Levelized cost of energy (LCoE) is commonly applied to tidal technologies. Ref. [23] provides detailed LCoE analyses, noting that although capital costs are high, operational savings and price stability render tidal energy financially competitive.

Research by Refs. [6,24] explores tidal stream economics within hybrid systems but identifies gaps in detailed models that integrate tidal energy, storage, and other renewables in regional contexts. They highlight that combining tidal with short-term storage yields unique benefits beyond traditional LCoE assessments.

The authors of [25] present a life cycle and economic evaluation of a 34.5 MW tidal farm consisting of 23 second-generation devices, estimating an LCoE of 0.125 EUR/kWh, consistent with European Commission projections. While informative for medium-scale projects, it omits systemic impacts of large-scale tidal integration on grid operations and the broader energy mix, which is an important gap.

Hydrogen is gaining prominence as a decarbonization enabler in hard-to-electrify sectors, serving both as energy storage and a clean fuel [12]. Green hydrogen produced by renewables, particularly tidal energy, promises enhanced system flexibility and efficiency [26,27]. However, long-term planning frameworks explicitly coupling tidal generation and hydrogen storage remain limited and require further development.

Traditional renewable expansion planning under uncertainty employs robust optimization [28,29] and integrated multi-energy models [30,31]. Many, however, lack flexibility for multi-year adaptation, relying on classical two-stage stochastic programming, which restricts their applicability in dynamic, uncertain contexts. While participatory scenario building represents an established approach for addressing deep uncertainty through stakeholder engagement, the IGDT framework was selected for this study due to its ability to provide quantifiable robustness guarantees for infrastructure investments under severe uncertainty without requiring precise probability distributions. This characteristic is particularly valuable for long-term power system planning, where stakeholder consensus on probability distributions may be unavailable and where decision-makers prioritize robustness against worst-case scenarios over probabilistic optimality.

This study addresses these limitations by proposing IG-FRM-TSP, combining IGDT with a flexible multi-period revision structure. This framework robustly manages deep uncertainties, allows plan adjustments across multiple planning horizons, and supports dynamic updates as new information emerges—essential for evolving energy landscapes.

To overcome the computational complexity of IG-FRM-TSP, a hybrid solution method is developed, integrating a modified Progressive Hedging algorithm with machine learning enhancements. Adaptive Progressive Hedging techniques—including adaptive penalty tuning, scenario bundling, and randomized scenario selection [32,33]—are

paired with machine learning for scenario reduction, parameter tuning, and warm-start initialization, significantly improving scalability and efficiency for multi-period planning involving tidal and hydrogen storage.

Key contributions of this paper include:

1. Development of a comprehensive framework integrating tidal energy into long-term planning, capturing its predictability and complementarity with renewables to reduce dispatch down and enhance flexibility within net-zero goals.
2. Introduction of a novel methodology combining IGDT and FRM-TSP, robustly addressing deep uncertainties and enabling adaptive plan revisions, including dynamic hydrogen storage interactions.
3. Construction of a scalable modeling framework assessing coordinated integration of tidal, offshore wind, and short- and long-term storage—including hydrogen—tailored for Northern Ireland. The framework evaluates CO_2 reductions and viability toward a resilient low-carbon system.
4. Explicit incorporation of CO_2 costs within IGDT-FRM-TSP, optimizing renewable integration and minimizing curtailment through improved supply–demand balance.
5. Implementation of an advanced hybrid solution enhancing progressive hedging with adaptive techniques and machine learning-driven scenario management, enabling scalable solutions for complex tidal integration problems.

By addressing these elements, this paper bridges key gaps in power system planning literature, especially the limited inclusion of tidal and hydrogen storage in net-zero-aligned expansion models.

The paper is structured as follows: Section 2 details the materials and methods. Section 3 discusses site selection and integration criteria. Section 4 presents the mathematical model. Section 5 describes the solution approach. Section 6 presents case studies and results, focusing on Northern Ireland's net-zero goals. Section 7 concludes with findings, policy implications, and recommendations for future research.

2. Materials and methods

This section details the framework employed in developing a techno-economic model for achieving net-zero emissions in Northern Ireland, focusing on energy transition pathways for the future power system. The study integrates renewable energy sources—wind (offshore and onshore), solar and tidal energy—while considering energy storage options, heating electrification, and CO_2 emission reduction. Although the present case study focuses on Northern Ireland, the proposed IG-FRM-TSP framework and its hybrid solution algorithm are jurisdiction-independent. The methodology can be directly transferred to other coastal or islanded systems with tidal resources. Only the input datasets (demand, renewable profiles, techno-economic parameters, and network constraints) are location-specific, whereas the model structure and optimization framework remain unchanged.

2.1. Model framework

The power system model presented in this paper incorporates the power system, hydrogen storage, and the electrification of heat demand as a scenario for electricity demand, as shown in Fig. 1. This model adopts a holistic approach to power system analysis, emphasizing the interconnections and synergies among various renewable energy technologies and ESSs. At the core of the model lies the power network, which interfaces with hydrogen storage through conversion technologies. Renewable energy sources, particularly tidal and offshore wind, play a pivotal role in this system. These intermittent sources can be directly utilized for power generation or converted to hydrogen via electrolysis units. Fuel cells enable bidirectional energy flow between hydrogen and power networks, converting hydrogen back to electricity when required. This capability enhances system flexibility and facilitates

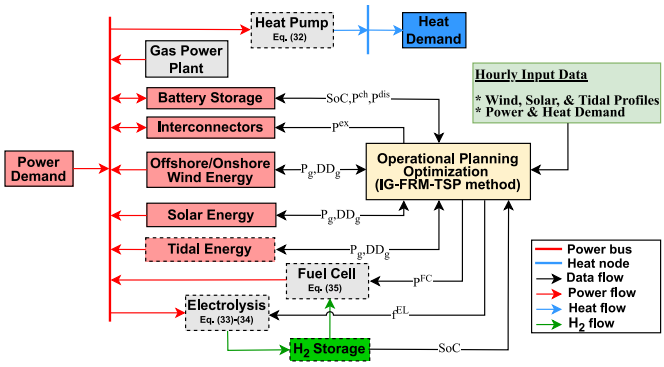

Fig. 1. Schematic of network technologies and interconnections with the power grid.

long-term energy storage, addressing the intermittency challenges associated with high renewable penetration. Energy storage plays a crucial role in this model. The model incorporates both short-term (battery energy storage) and long-term (hydrogen storage) options. These storage technologies are pivotal in scenarios with high renewable penetration, particularly in balancing the variability of tidal and offshore wind resources. It is important to note that this model focuses on transmission-level dynamics, aggregating generation units and demands at this higher level. Lower-level network details and associated losses are omitted and the model's focus is maintained on high-level system interactions and planning scenarios. A key objective of this study is to determine optimal storage solutions in the context of high renewable penetration, with a particular emphasis on tidal energy and offshore wind integration. Furthermore, the model aims to elucidate the most effective pathways to achieve net zero emissions targets. A mixed-integer linear programming (MILP) model is developed to optimize the power system planning for Northern Ireland, focusing on minimizing total system costs while ensuring that the system adheres to CO_2 emission reduction targets. The objective is to minimize the total system cost across the planning horizon, including investment costs, operational costs, CO_2 emission costs, and dispatch down penalty.

To provide an integrated overview of the methodology, a schematic flowchart of the study framework is presented in Fig. 2. This diagram summarizes the major input datasets, the scenario generation and reduction process, the IG-FRM-TSP optimization structure, and the final outputs, including validation in DIgSILENT. It highlights the overall workflow of the study and bridges the gap between the system representation and the optimization algorithm. The scenario generation process in Fig. 2 follows a structured four-stage approach:

1. **Historical Data Collection**: Establishment of the baseline using System Operator of Northern Ireland (SONI) operational data and project-specific site measurements (e.g., X-Flow tidal data).
2. **Stochastic Perturbations**: Creation of multiple plausible trajectories capturing both inter-annual variability and forward-looking policy and technology developments.
3. **Uncertainty Bound Definition**: Application of deep uncertainty ranges from Table 4 to define the comprehensive uncertainty space.
4. **Computational Optimization**: Use of K-means clustering to reduce computational complexity while preserving representative variability across demand, resource, cost, and policy dimensions.

This structured approach ensures comprehensive coverage of the uncertainty space while maintaining computational tractability for multi-period optimization, directly addressing the scenario generation component illustrated in Fig. 2.

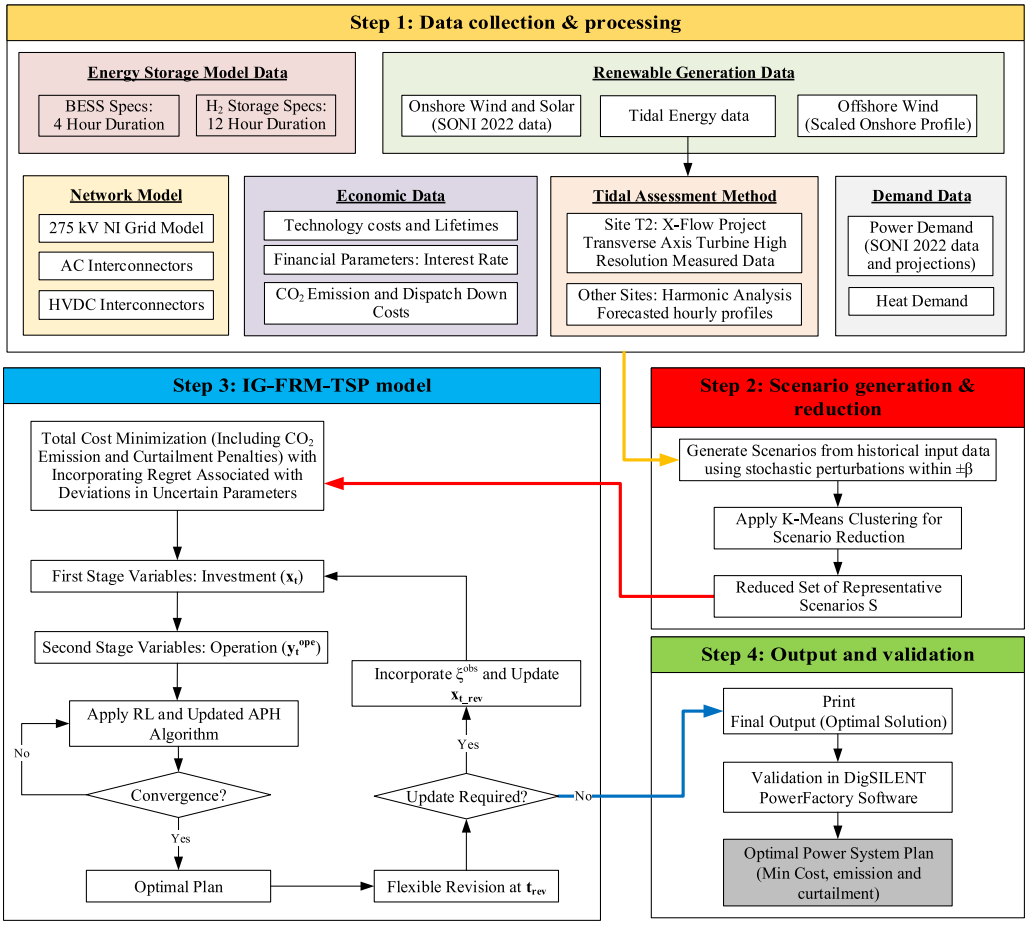

Fig. 2. Overall framework of the proposed IG-FRM-TSP methodology for power system planning under deep uncertainty.

2.2. Energy storage modeling

To assess the role of energy storage in supporting renewable integration, the model incorporates both short-term and long-term energy storage solutions:

1. Battery energy storage is modeled for short-term energy storage, with a cycle duration of 4 hour. This is particularly useful for intra-day balancing and managing short-term fluctuations in renewable energy output.
2. Hydrogen storage is modeled as a long-term energy storage solution, with a cycle duration of 12 hour. This allows for daily storage needs, helping to balance supply and demand over longer periods and potentially reducing curtailment of renewable energy sources.

Hydrogen storage is included in this model due to its unique ability to store large quantities of energy for extended periods. This capability is crucial for addressing seasonal variations in renewable energy production and demand, which cannot be effectively managed by short-term storage solutions alone. Furthermore, hydrogen storage can play a vital role in sector coupling, allowing excess renewable electricity to be converted into hydrogen for use in other sectors such as industry or transportation, thus providing additional flexibility to the overall energy system.

2.3. Electrification of heating

The transition to low-carbon heating systems is crucial for reducing CO_2 emissions in Northern Ireland's residential and commercial sectors. A significant proportion of buildings in Northern Ireland still rely on fossil fuel-based heating systems, presenting both a challenge and an opportunity for decarbonization. According to the International Energy Agency (IEA), heat pumps can reduce greenhouse gas emissions by at least 20 % compared to gas boilers, even when running on emissions-intensive electricity [34]. This reduction can be as high as 80 % in countries with cleaner electricity grids. Authors in Ref. [13] demonstrated the significant potential of heat pump electrification in a wind-dominated market, showing that it can deliver at least two to three times fewer carbon emissions compared to conventional heating options such as gas or oil. Their study of the Irish all-island electricity market, which shares similarities with Northern Ireland's energy landscape, revealed that energy storage systems combined with heat pumps could deliver substantial benefits in terms of carbon emission reduction and energy system flexibility. While [13] focused on wind power, the principles can be extended to tidal energy, which offers the advantage of being more predictable than wind. The electrification of heating in this paper is modeled through the adoption of heat pumps, which represent a key strategy for reducing CO_2 emissions. By simulating this scenario, the potential for CO_2 emission reductions through heating electrification is explored, and the broader implications for Northern Ireland's energy infrastructure are discussed.

3. Potential site selection and renewable integration

Northern Ireland's marine resources present substantial potential for renewable energy development. A Strategic Environmental Assessment (SEA) conducted by the Energy and Climate Change Committee identified capacities of 900 MW for offshore wind and 300 MW for tidal

stream energy by 2020, with minimal environmental impact [35]. These resource zones are predominantly situated along Northern Ireland's North West, Eastern, and North Eastern coasts. The assessment revealed a limited potential for wave energy off the north-west coast, which was considered unsuitable for commercial-scale development. Three smaller tidal resource zones-Strangford Lough, the Maidens, and Copeland Island - were identified as potential sites for pre-commercial or demonstration projects [35]. A comprehensive analysis of tidal stream energy resources in the UK and British Channel Islands [24] identified several prospective and speculative sites relevant to Northern Ireland, including areas under development, historically withdrawn plots, and potential future development zones. According to this reference, 5 zones for tidal energy are identified, with capacities varying among these zones. The largest zone has a confirmed capacity of 200 MW. The details of zones and capacities are introduced in Section 6. The spatial analysis of tidal energy resources in relation to the existing grid infrastructure offers valuable insights for future planning and integration of tidal energy into Northern Ireland's renewable energy portfolio.

3.1. Tidal energy integration

Tidal energy integration is grounded in high-resolution generation data from the X-Flow project, which features the Transverse Axis Crossflow Turbine (TACT) technology tested at the Queen's University Belfast Tidal Test Site. By leveraging detailed data from an on-site project, this approach provides an accurate generation profile that supports evaluating the system-wide impacts of tidal energy, specifically for reducing curtailment and improving grid stability.

For potential sites lacking comprehensive measurement data, predictive modeling was applied following the harmonic analysis methods outlined in Ref. [36]. This predictive approach involves generating hourly tidal profiles by forecasting tidal behavior over a year, including heights above mean sea level and current speeds at 0.5-hour intervals. For sites with partial or no recorded data, these projections ensure coverage across all possible candidate locations.

This study explores the integration of tidal energy using both a baseline and an ambitious scenario to evaluate its impact on grid stability and renewable generation profiles. The baseline scenario represents a practical capacity of 100 MW, reflecting a more achievable deployment of tidal energy by 2030. In contrast, the ambitious scenario considers a hypothetical capacity of 260 MW, which illustrates the potential for higher tidal penetration in the future. While the total viable tidal resource is estimated at 320 MW, achieving even the baseline scenario by 2030 may be challenging. Nevertheless, these scenarios provide valuable insights into the role of tidal energy in shaping future energy systems and policies. The ambitious scenario, in particular, enables an assessment of high tidal penetration's ability to contribute to flattening the overall generation profile of the power system, highlighting its long-term potential as part of a renewable energy strategy.

Technologies such as floating tidal stream platforms and tidal kite systems could offer substantial potential to increase tidal energy deployment in Northern Ireland by enabling access to deeper waters and stronger tidal currents that are not accessible to conventional fixed-bottom installations. Although an exhaustive assessment of Northern Ireland's expanded tidal potential remains an area for further research, the ambitious scenario provides a preliminary view of the possible benefits.

Where actual measurement data was available, it was incorporated directly to improve the model's accuracy. This dual approach—combining real data with advanced predictive methods—allows for robust and comprehensive modeling of tidal energy contributions, tailored to the site-specific characteristics across all candidate locations.

In the 100 MW scenario, it is assumed that the connection to the grid is facilitated via a 10 km subsea cable and a 275 kV overhead transmission line, as detailed in Section 6. For the 260 MW scenario, generation is connected through a similar configuration comprising a 10 km subsea cable and a 275 kV overhead transmission line. An additional ambitious scenario, which is not reflective of real-world expectations for 2030, is also considered to further explore the role of tidal energy in achieving net-zero targets. In this case, a total tidal capacity of 360 MW is assumed, with 260 MW connected as in the original configuration and the remaining 100 MW integrated into the 110 kV network at the 275 kV Castlereagh bus, as detailed in Section 6.

3.2. Wind offshore energy integration

Incorporating offshore wind into the model requires an approximation method, as high-resolution, site-specific offshore wind time-series are not publicly available for Northern Ireland. To represent offshore performance in a transparent and consistent way, this study scales the generation profile of the nearest coastal onshore site by 10 %. This increase is motivated by the well-documented performance gap between offshore and onshore wind farms: Multiple studies have shown that offshore sites in the UK and Europe achieve systematically higher capacity factors, typically in the range of 35 %–45 % compared with 20 %–30 % for onshore sites, due to higher mean wind speeds, lower turbulence intensity, and greater resource consistency over open water [37,38]. The 10 % adjustment therefore represents a deliberately conservative proxy that avoids overstating offshore performance, while ensuring that offshore wind's inherent advantage is not suppressed in the system planning analysis. To ensure robustness, two additional measures are applied. First, a sensitivity analysis is conducted in which the offshore uplift factor is increased beyond the baseline 10 % value, allowing the impact of stronger offshore assumptions on system behavior to be explored. Second, consistent with the treatment of other renewable technologies, offshore wind generation is incorporated within a structured uncertainty range of ± 15 % under the IGDT-FRM-TSP framework. These measures ensure that the simplified offshore wind representation is tested across a reasonable envelope of assumptions, and that the robustness of system-level insights is preserved despite the absence of site-specific offshore data. This standardized approach enables a balanced comparison of integration challenges for tidal and offshore wind resources. While the present study employs a conservative and robust proxy to represent offshore wind generation, a valuable avenue for subsequent research is the development of site-specific offshore wind profiles for Northern Ireland. This could be achieved through the use of high-resolution reanalysis datasets combined with bias correction and validation against observational measurements, following the approaches demonstrated in offshore wind modeling studies [39,40]. Such extensions would enable even more detailed assessments of offshore wind dynamics and their interactions with tidal resources in future planning analyses. For consistency with the tidal energy modeling assumptions, offshore wind plants are connected to the grid via a 10 km subsea cable and a 275 kV overhead transmission line, as detailed in Section 6.

3.3. Wind onshore and solar energy integration

To accurately model onshore wind and solar energy, the generation profiles are tailored for each 275 kV node of the Northern Ireland grid, using data from the SONI for the year 2022. This dataset provides high-resolution information on the connected onshore wind and solar installations, allowing for node-specific generation profiles to be developed and incorporated into the model. By aligning generation data with the geographic distribution of renewable resources at each node, the model can more accurately represent the unique generation patterns across Northern Ireland's grid. This approach enhances the model's reliability, particularly in assessing the impacts of renewable integration on system stability, curtailment minimization, and grid flexibility.

4. Mathematical formulation

This paper proposes the novel IG-FRM-TSP method for power system planning under deep uncertainties involving demand growth, renewable

generation, interest rates, policy changes and technology costs. While long-term climate change projections are beyond the scope of this study, climate-related uncertainties are indirectly captured within the deep uncertainty parameters. The IGDT framework's robustness analysis ensures that planning decisions remain viable across a wide range of potential climate-influenced futures, including worst-case scenarios that may arise from climate impacts on demand patterns and renewable resource availability. The IGDT is a non-probabilistic approach for decision-making in the face of severe uncertainty, as outlined by Ref. [41,42]. The IG-FRM-TSP framework provides a robust and adaptive planning approach which can address the complexities and uncertainties of the long-term planning problem with net-zero targets. The mathematical formulation of IG-FRM-TSP builds upon these foundational approaches and is detailed in the following sections.

4.1. IG-FRM-TSP framework

The objective function in the IG-FRM-TSP framework aims to minimize the expected total costs while incorporating regret associated with deviations in uncertain parameters and to maximize robustness. It is formulated as follows:

$$\min \ \mathbb{E}\left[C^{total}\right] + \lambda \,\mathrm{Regret}_{max} - \mu\, \alpha^* \tag{1}$$

where $\mathbb{E}\left[C^{total}\right]$ represents the expected total cost across all probabilistic scenarios, including investment, operational, and penalty costs. λ is a weight factor applied to the maximum regret, balancing cost-efficiency with resilience. Regret_{max} denotes the maximum regret related to deviations in key uncertain parameters. μ is a weight factor applied to the robustness measure. α^* is the robustness function from IGDT, as defined in Eq. (3).

4.2. IGDT-based robustness under deep uncertainty

Deep uncertainty refers to situations where decision-makers cannot agree on a single probabilistic model for key system parameters, often due to long time horizons, lack of data, or the potential for disruptive changes. In this study, deep uncertainty encompasses demand growth, technology costs, fuel prices, and CO_2 policy.

To model robustness under this deep uncertainty, an uncertainty set $\mathcal{U}(\bar{\alpha})$ is constructed. This set defines the plausible range of deviation from the nominal values $\hat{\xi}_{i,t}$ for each key uncertain parameter i (e.g., demand D_t, renewable generation G_t, interest rates r_t, policy variables p_t). The maximum possible deviation for each parameter is defined by a parameter-specific bound β_i (see Table 4). The uncertainty set for a given common horizon $\bar{\alpha}$ is then defined as:

$$\mathcal{U}(\bar{\alpha}) = \left\{ \xi_{i,t} \ : \ \frac{|\xi_{i,t} - \hat{\xi}_{i,t}|}{|\hat{\xi}_{i,t}|} \le \bar{\alpha} \cdot \beta_i, \ \forall i \in \mathcal{I}, \ \forall t \in \mathcal{T} \right\}. \tag{2}$$

Here, $\bar{\alpha} \ge 0$ is a scaling factor that uniformly expands or contracts the uncertainty bounds for all parameters. The parameter-specific β_i values, which can be asymmetric (e.g., $\beta_i \in [-a, b]$), ensure the model captures the unique characteristics of each uncertainty source.

The IGDT robustness function α^* identifies the maximum horizon $\bar{\alpha}$ such that the system remains feasible and acceptable under the worst-case realization of uncertainties within $\mathcal{U}(\bar{\alpha})$:

$$\alpha^* = \max_{\bar{\alpha} \ge 0} \left\{ \bar{\alpha} \ : \ \max_{\xi \in \mathcal{U}(\bar{\alpha})} C^{total}(\xi) \le C_{\mathrm{th}} \right\}, \tag{3}$$

where $C^{total}(\xi)$ denotes the total system cost under realization ξ, and C_{th} is the maximum acceptable cost level. This formulation explicitly evaluates the worst-case system response, thereby ensuring robustness in a non-probabilistic manner. The value α^* is a direct output of this optimization, representing the largest uncertainty horizon the system can tolerate.

The integration of IGDT with the FRM-TSP model modifies the first-stage planning problem by embedding the uncertainty set $\mathcal{U}(\bar{\alpha})$ into the feasibility constraints. Investment and operational decisions must therefore remain feasible for all realizations $\xi \in \mathcal{U}(\bar{\alpha})$. The hybrid optimization problem can be expressed as:

$$\min_{x,y} \ \mathbb{E}_{s \in S}\left[C^{stoch}(x, y; \xi_s)\right] \quad \text{s.t.} \quad (x, y) \in \mathcal{F}(\xi), \ \forall \xi \in \mathcal{U}(\bar{\alpha}), \tag{4}$$

where $C^{stoch}(x, y; \xi_s)$ is the expected stochastic cost under scenario s, and $\mathcal{F}(\xi)$ denotes the feasible set of operational constraints given realization ξ. In this hybrid structure, the stochastic component addresses policy and market uncertainties where probabilistic information is available, while the IGDT component guarantees robustness by ensuring feasibility against all non-probabilistic deviations in $\mathcal{U}(\bar{\alpha})$.

The robustness value α^* provides a direct measure of system tolerance to deep uncertainty. A low α^* indicates a plan is only robust to small variations around the nominal forecast. A high α^* indicates the plan can withstand larger, more disruptive shocks, such as those caused by technological breakthroughs, severe climate impacts, or sudden policy shifts. The ranges for the deviation bounds β_i (provided in Table 4) are based on literature and expert judgment to encompass these potential futures. Thus, the IGDT framework, through the calculation of α^*, operates as a form of Robust Decision-Making (RDM) by stress-testing strategies against a vast space of plausible futures to identify those that are robust across many of them.

4.3. FRM-TSP framework

The IG-FRM-TSP framework introduces two sets of decision variables to enable adaptive multi-period planning:

- **First-stage variables** (x_t): These represent long-term investment decisions, made prior to the realization of uncertainty.
- **Second-stage variables** (y_t^{ope}): These represent operational adjustments that are made after uncertainties, such as demand or renewable generation, are realized.

To implement the adaptive multi-period planning approach, the following constraints are introduced:

$$x_N \in X_t(x_{t-1}, B_t) \quad \forall t \in \mathcal{T} \tag{5}$$

Eq. (5) ensures that the first-stage investment decisions x_t are feasible given the previous period's decisions x_{t-1} and the available budget B_t for each network at time period t.

$$y_t^{\mathrm{ope}} \in Y_{s,t}(x_t, \xi_s) \quad \forall t \in \mathcal{T}, s \in S \tag{6}$$

The constraint in Eq. (6) defines the feasible set for second-stage operational decisions $y_{N,t}^{ope}$ based on the first-stage decisions x_t and the realized uncertainties ξ_s for each time period t and scenario s.

$$x_t = x_t^{\mathrm{initial}} \quad \forall t < t_{\mathrm{rev}} \tag{7}$$

$$x_t \in X_t^{\mathrm{rev}}(x_{t-1}, \xi^{obs}, B_t) \quad \forall t \ge t_{\mathrm{rev}} \tag{8}$$

Constraints in Eqs. (7) and (8) implement the revision mechanism. For periods before the revision time t_{rev}, decisions follow the initial plan. After t_{rev}, decisions are updated based on observed uncertainties ξ_{obs} and the available budget.

The IG-FRM-TSP framework follows a two-stage stochastic approach to accommodate multi-period decision-making under uncertainty:

1. Investment decisions: Investment costs are constrained by a total budget B^{Inv} over the planning horizon as expressed in Eq. (9).

$$\sum_{t \in \mathcal{T}} \left(\sum_{g \in \Omega^g} x_{g,t} C_g^{Inv} + \sum_{st \in \Omega^{st}} x_{st,t} C_{st}^{Inv} \right) \le B^{Inv} \tag{9}$$

2. Operational adjustments: Operational costs are adjusted according to the realized uncertainties in each time period t as expressed in Eq. (10), ensuring that the system adapts flexibly.

$$y_t^{\text{ope}} = f\left(x_t, D_t, G_t, r_t, p_t\right) \tag{10}$$

where f is a function of first-stage investments and realized uncertainties.

4.4. Quantifying policies for multi-criteria impact

Policies play a crucial role in shaping the behavior of energy systems. These can be quantified by integrating them as economic incentives, costs, or constraints within the model. Policies are typically deliberate guidelines or regulations designed to influence decision-making, foster certain outcomes, or impose restrictions on energy markets. While the policies themselves are not random, their implementation can drive changes in various model parameters, creating uncertainty or variability that impacts the system's behavior. Thus, policies are modeled as parameters that modify inputs or constraints in a structured manner.

4.4.1. Tidal energy incentive

A key policy for promoting renewable energy generation involves incentivizing the output of offshore wind and tidal energy. To model this, a subsidy scheme can be applied, which scales with the energy produced. The subsidy could be expressed per unit of generated energy, incentivizing higher production levels, particularly during peak demand periods. This dynamic structure ensures that the subsidy is responsive to system needs, encouraging more generation when required.

Mathematically, the tidal energy incentive can be incorporated using a subsidy multiplier. The subsidized investment cost for tidal energy generation is calculated by adjusting the original investment cost based on the subsidy factor, which can vary over time. This approach is shown in the following equation:

$$C_g^{Inv,subsidized} = C_g^{Inv}\left(1 - Sub_t^{Tidal}\right), \quad \forall g \in \Omega^{Tidal} \tag{11}$$

where $C_g^{Inv,subsidized}$ is the subsidized investment cost for tidal energy that would replace the tidal investment cost when the subsidy is applied in the model.

4.4.2. Net-zero emission policy

To align with global efforts toward decarbonization, carbon pricing mechanisms can be incorporated into the model as a policy tool. The net-zero emission policy aims to drive emissions reductions by imposing a cost for carbon emissions, which incentivizes cleaner energy technologies. Rather than treating the CO_2 cost as a fixed value, the policy-driven approach uses a progressive carbon pricing system that increases with higher emission levels. This dynamic system encourages the deployment of low-emission technologies and penalizes higher emissions.

A tiered CO_2 pricing structure can be implemented within the model, where the CO_2 price increases as emissions exceed certain thresholds, reflecting the regulatory risk of non-compliance and motivating stricter emission control measures. The pricing structure can be defined mathematically as follows:

$$C^{CO_2} = \begin{cases} C_t^{CO_2}, & \text{if } e_t^{CO_2} \le \text{cap}_{\text{low}} \\ \delta_1\, C^{CO_2}, & \text{if } \text{cap}_{\text{low}} < e_t^{CO_2} \le \text{cap}_{\text{high}} \\ \delta_2\, C^{CO_2}, & \text{if } e_t^{CO_2} > \text{cap}_{\text{high}} \end{cases} \tag{12}$$

where δ_1 and δ_2 are escalation factors representing higher penalties for exceeding emissions caps.

4.5. Objective function

The objective function seeks to minimize the total system costs, which include investment, operational, emission, and dispatch-down costs. Eq. (13) calculates the aggregate system cost by summing these four components across all time periods t. In this equation, the term $\lambda \cdot \text{Regret}_{\max}$ represents a risk-averse approach by minimizing the maximum regret, while the term $\mu \cdot \alpha^*$, which includes the confidence level α^*, is used to control the probability of achieving specified outcomes.

$$C^{total} = \min \sum_{s\in S} p_s \left\{ \sum_{t\in\mathcal{T}} \left(\text{AF}_{s,T}\left(x_{g,t} R_g C_g^{Inv} + x_{st,t} R_{st} C_{st}^{Inv} + C_s^{Ope} \right) + e_t^{CO_2} C_s^{CO_2} + \sum_{g\in\Omega^{Re}} c_s^{DD}\, DD_{g,t} \right) \right\} + \lambda\, \text{Regret}_{\max} - \mu\, \alpha^* \tag{13}$$

The annualization factor, $AF_{s,t}$, is calculated using Eq. (14).

$$\text{AF}_{s,t} = \frac{r_s (1+r_s)^t}{(1+r_s)^t - 1} \tag{14}$$

The operational costs, defined as the sum of fixed and variable operational costs, are represented by Eq. (15). To account for policy uncertainty, these operational costs are expressed in terms of various scenarios that reflect potential future policies affecting costs and operational decisions. The costs associated with these policies are computed as detailed in Eq. (15).

$$C_s^{Ope} = OC^F + OC^V \tag{15}$$

Eq. (16) represents fixed operational costs for generation and storage units. While Eq. (17) details variable operational costs. The variable operational costs include contributions from various energy sources and reflect adjustments based on policy changes.

$$OC^F = \left(\sum_{g\in\Omega_g} OC_g^F + \sum_{st\in\Omega_{st}} OC_{st}^F \right) \tag{16}$$

$$OC^V = \sum_{t\in\mathcal{T}} \left(c^{elec} P_{E,g,t} + c^{gas} f_{G,g,t} \right) \tag{17}$$

4.6. Power system model

The model operates under several constraints to ensure system stability and reliability. The power balance constraint is given by Eq. (18) which represents the power balance constraint for each bus i at time t. Reactive power balance is maintained by Eq. (19). The AC power flow mathematical model and constraints presented in this work are established from the linearized model developed in Ref. [43].

$$\sum_{g\in\Omega g} P_{i,g,t} + \sum_{i\in\Omega^{Co}} P_{i,t}^{ex} - \sum_{st\in\Omega^{st}} (P_{i,st,t}^{ch} - P_{i,st,t}^{dis}) - P_{i,t}^{D} = P_{i,t}^{inj} \tag{18}$$

$$\sum_{g\in\Omega_g} Q_{i,g,t} + \sum_{i\in\Omega_{Co}} Q_{i,t}^{ex} - Q_{i,t}^{D} = Q_{i,t}^{inj} \tag{19}$$

Eqs. (20) and (21) represent the linearized AC power flow model for active and reactive power injections at each node in the power system. Eqs. (22) and (23) represent active and reactive power flow between buses i and j. Voltage limits are enforced by Eq. (24) ensures voltage levels remain within specified limits. Active and reactive power generation limits are defined by Eqs. (25) and (26) which ensures generation remains within capacity limits.

$$P_{i,t}^{inj} = -(2V_{i,t} - 1)B_{ii}^{y} + \sum_{j\in\Omega^n, j\neq i} (\theta_{i,t} - \theta_{j,t}) G_{ij}^{y} - \sum_{j\in\Omega_n} (V_{i,t} + V_{j,t} - 1) B_{ij}^{y} \tag{20}$$

$$Q_{i,t}^{inj} = (2V_{i,t} - 1)G_{ii}^{y} + \sum_{j\in\Omega_E^n, j\neq i} (\theta_{i,t} - \theta_{j,t}) B_{ij}^{y} + \sum_{j\in\Omega_E^n} (V_{i,t} + V_{j,t} - 1) G_{ij}^{y} \tag{21}$$

$$P_{ij,t} = G_{ij}(V_{i,t} - V_{j,t}) - B_{ij}(\theta_{i,t} - \theta_{j,t}) \tag{22}$$

$$Q_{ij,t} = -B_{ij}(V_{i,t} - V_{j,t}) - G_{ij}(\theta_{i,t} - \theta_{j,t}) \tag{23}$$

$$\underline{V}_i \le V_{i,t} \le \overline{V}_i \tag{24}$$

$$\underline{P}_g \le P_{i,g,t} \le \overline{P}_g \tag{25}$$

$$\underline{Q}_g \le Q_{i,g,t} \le \overline{Q}_g \tag{26}$$

Eq. (27) ensures transmission line flows remain within capacity limits.

$$\underline{P}_{ij} \le P_{ij,t} \le \overline{P}_{ij} \tag{27}$$

4.7. Energy storage modeling

The integration of energy storage systems is crucial for managing the variability of renewable energy sources and enhancing system flexibility. This model incorporates both short-term (batteries) and long-term (hydrogen) storage options, each playing a distinct role in balancing supply and demand across different timescales. The energy storage model is based on the framework presented in Ref. [44], with adaptations to accommodate both battery and hydrogen storage systems. The following equations describe the dynamics and constraints of the storage systems. Eq. (28) represents the state of charge (SoC) evolution for storage system s at time t. It accounts for the previous SoC, charging input, and discharging output, considering the respective efficiencies.

$$SoC_{st,t} = SoC_{st,t-1} + \frac{\eta_{st}^{ch} P_{st,t}^{ch} \Delta t}{\overline{P_{st}}} - \frac{P_{st,t}^{dis} \Delta t}{\eta_{st}^{dis} \overline{P_{st}}} \tag{28}$$

Eq. (29) enforces the operational limits on the SoC, ensuring it remains within the specified range.

$$\underline{SoC}_{st} \le SoC_{st,t} \le \overline{SoC}_{st} \tag{29}$$

Eqs. (30) and (31) limit the charging and discharging powers, respectively, based on the storage capacity and operational status.

$$0 \le P_{st,t}^{ch} \le \overline{SoC}_{st}\, \overline{P}_{st}\, x_{st,t}^{ch} \tag{30}$$

$$0 \le P_{st,t}^{dis} \le \underline{SoC}_{st}\, \overline{P}_{st} (1 - x_{st,t}^{ch}) \tag{31}$$

For battery storage, these equations are applied with a cycle duration of 4 hour, reflecting its role in short-term energy balancing. For hydrogen storage, the same equations are used, but with the power terms (P) replaced by hydrogen flow terms (f), and a cycle duration of 12 hour is considered, representing its capacity for longer-term energy storage. Eqs. (32) and (33) relate the hydrogen storage charging and discharging to the electrolyzer and fuel cell operations, respectively, where LHV_{H2} is the lower heating value of hydrogen.

$$f_{st,t}^{H2,ch} = \eta^{EL} P_{st,t}^{EL} / LHV_{H2} \tag{32}$$

$$P_{st,t}^{FC} = \eta^{FC} f_{st,t}^{H2,dis} LHV_{H2} \tag{33}$$

4.7.1. Heat pump

The heat pump model, adapted from [44], relates the electrical power consumption to the thermal power output as expressed in Eq. (34).

$$P_{Th,t}^{HP} = P_{i,t}^{D,HP}\, COP\, \eta^{HP} \tag{34}$$

where $P_{i,t}^{D,HP}$ is the electrical power consumed by the heat pump at node i and time t and $P_{Th,t}^{HP}$ is the thermal power output at time t.

4.7.2. Alkaline electrolyzer

The electrolyzer model, as presented in Ref. [45], converts electrical power into hydrogen, as described by Eq. (35). The electrolyzer operation is constrained by its capacity, denoted as $\overline{P}^{D,EL}$, which is expressed in Eq. (36).

$$f_t^{EL} = \frac{1}{LHV_{H2}} \eta^{EL} P_{i,t}^{D,EL} \tag{35}$$

$$0 \le P_t^{D,EL} \le \overline{P}^{D,EL} \tag{36}$$

where f_t^{EL} is the hydrogen production rate.

4.7.3. Fuel cell

The fuel cell model, as detailed in Ref. [45], facilitates the conversion of hydrogen into electricity, enabling efficient energy utilization within the integrated energy system. This process is mathematically represented in Eq. (37).

$$P_{i,t}^{FC} = \eta^{FC} f_t^{D,FC} LHV_{H2} \tag{37}$$

where $P_{i,t}^{FC}$ is the electrical power output and $f_t^{D,FC}$ is the hydrogen consumption rate.

4.8. Dispatch down

The DDRI serves as a key metric to assess and monitor renewable energy curtailment relative to available renewable generation, allowing the model to evaluate dispatch strategies that maximize renewable utilization and support cleaner energy integration. This index, defined in Eq. (38), measures dispatch down as a normalized share of curtailed renewable energy relative to the available renewable generation for each renewable source g over time periods t:

$$DDRI = \frac{\sum_{t\in\mathcal{T}} \sum_{g\in\Omega_{Re}} DD_{g,t}}{\sum_{t\in\mathcal{T}} \sum_{g\in\Omega_{Re}} Avail_{g,t}}, \qquad 0 \le DDRI \le 1 \tag{38}$$

where $DD_{g,t}$ is the curtailed energy of renewable source g at time t, and $Avail_{g,t}$ is its available generation. By construction, DDRI is a normalized indicator: a value of 0 indicates no dispatch down, while a value of 1 indicates full curtailment of all available renewable generation. In scenarios with high renewable variability due to fluctuating weather conditions and operational constraints, DDRI provides a systematic approach to examine curtailment and renewable absorption. Lower DDRI values reflect more effective integration of renewables, aligning with sustainability goals and advancing the transition toward a low-carbon energy system.

The System Non-Synchronous Penetration (SNSP) limit is critical for managing renewable dispatch levels. It constrains the proportion of non-synchronous generation within the grid to maintain stability while progressively increasing renewable penetration. Following the SONI operational definition, SNSP is currently limited to 75 %, with strategic increments planned to reach 95 % by 2030. SNSP is therefore a key factor in grid flexibility and renewable dispatch management, and is formulated as:

$$SNSP_t = \frac{\sum_{g\in\Omega_{Re}} P_{g,t} + P_t^{HVDC,imp} + P_{st,t}^{dis}}{\sum_{i\in\Omega_n} P_{i,t}^{D}} \le \overline{SNSP} \tag{39}$$

where $P_t^{HVDC,imp}$ is imported power via HVDC links. In the high-renewable scenarios considered in this study, batteries primarily charge from surplus renewable energy during low-demand periods. Therefore, including $P_{st,t}^{dis}$ in the numerator reasonably represents time-shifted non-synchronous supply, supporting renewable absorption while maintaining stability within the SNSP constraint.

Eq. (39) ensures that, at any given time t, the share of non-synchronous generation does not exceed the predefined SNSP limit $\overline{SNSP}$. This constraint is essential for grid stability and directly influences dispatchable capacity, reducing dispatch-down events while allowing greater levels of renewable integration within stability limits.

5. Solution methodology

Given the complexity of the IG-FRM-TSP model, which requires adaptive and robust handling of multi-period uncertainties, this paper proposes an advanced hybrid approach. The methodology combines the APH algorithm with ML enhancements to efficiently solve multi-stage stochastic programs, addressing both significant computational demands and uncertainties.

The proposed methodology incorporates developments in APH, including adaptive penalty adjustment, scenario bundling, and randomized scenario handling, which have been shown to improve convergence and efficiency in large-scale applications [32,33]. ML techniques for scenario reduction, parameter tuning, and efficient warm-starting of decision variables, further optimizing the algorithm's performance are integrated. These innovations allow the proposed method to effectively address the flexibility and robustness requirements of the IG-FRM-TSP model, enhancing both solution accuracy and computational efficiency. The solution framework for the proposed IG-FRM-TSP model is illustrated in Fig. 3. The decision-making process is divided into two primary stages: Planning Decisions (Stage 1) and Operational Decisions (Stage 2). Stage 1 corresponds to first-stage investment variables ($x_{g,t}, x_{st,t}$), such as capacity expansion of generation and storage, defined in Eqs. (5), (7)–(9). Stage 2 corresponds to second-stage operational variables (y_t^{ope}), including generation dispatch ($P_{g,t}$), storage operation ($P_{st,t}^{ch}$, $P_{st,t}^{dis}$), curtailment ($DD_{g,t}$), and network flows ($P_{ij,t}, Q_{ij,t}$), as described in Eqs. (6) and (10). Revision points (R_1–R_5) represent the adaptive update mechanism from Eqs. (7) and (8), where observed uncertainties in demand, technology costs, renewable output, or CO_2 pricing trigger revisions of both planning and operational paths.

The timeline progresses across distinct time steps (t_0 to t_5), with revision points (R_1 to R_5) marking opportunities for adaptive changes based on observed uncertainties. At revision time t_2, for example, R_3 incorporates newly observed uncertainty, leading to updated decision trees. These trees are refined using k-means clustering and IGDT, which categorize regions as safe, risky, or unknown. Neural network warm starts and reinforcement learning (RL) with adaptive clustering contribute to refining initial solutions, facilitating optimal decision-making by dynamically adjusting penalty parameters γ in the APH algorithm. Specifically, RL observes the convergence trajectory of APH, treats each iteration's convergence status as a state, and adjusts γ as an action, with faster convergence and lower residuals serving as the reward signal. This adaptive tuning avoids over-penalization and ensures convergence stability in large-scale uncertain environments. Finally, the framework identifies the optimal decision path that aligns with net-zero objectives while minimizing risk and cost.

5.1. APH algorithm

To solve the multi-stage stochastic programming model, an APH algorithm is adopted, incorporating bundle and adaptive tuning methods. The updated APH steps are as follows:

1. **Initialization**: Set the iteration counter $k = 0$, and initialize decision variables $x_{s,t}^0$ for each scenario s and time period t. Select an initial penalty parameter γ_0 and a clustering threshold for scenario grouping.
2. **Scenario Bundling and Subproblem Solving**: For each scenario group (or "bundle"), which represents related uncertainty paths, solve the subproblem:

$$\min_{x_{s,t}} \sum_{t\in\mathcal{T}} f_{s,t}(x_{s,t}) + \gamma \sum_{t\in\mathcal{T}} \|x_{s,t} - \bar{x}_t^k + w_{s,t}^k\|^2 \tag{40}$$

   where $\bar{x}_t^k$ is the average solution across scenarios in each bundle, and $w_{s,t}^k$ are penalty terms. This approach improves solution stability and convergence when facing weakly convex or non-convex objectives.
3. **Update Scenario Averages and Penalties**: Calculate updated scenario averages $\bar{x}_t^{k+1}$ across each scenario bundle, and adapt penalties as:

$$w_{s,t}^{k+1} = w_{s,t}^k + \gamma(x_{s,t}^{k+1} - \bar{x}_t^{k+1}). \tag{41}$$

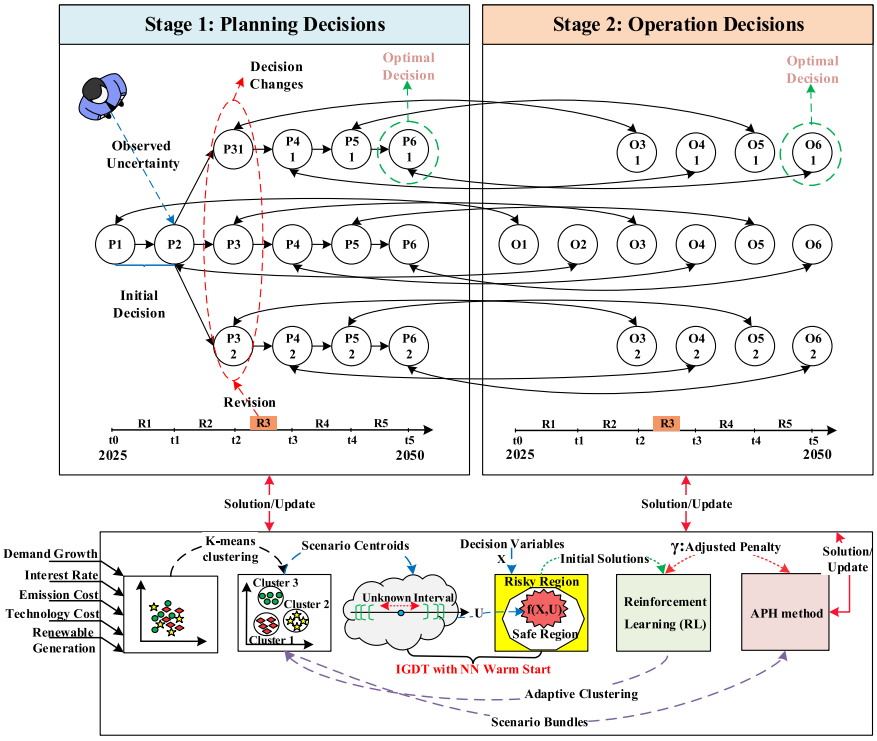

Fig. 3. An illustration of IG-FRM-TSP solution methodology.

4. **Adaptive Penalty Parameter Tuning**: Adjust γ dynamically based on convergence metrics, informed by RL. This enables faster convergence, particularly in highly uncertain environments, and mitigates over-penalization.
5. **Convergence Check**: If $\|x_{s,t}^{k+1} - \bar{x}_t^{k+1}\| < \epsilon$ for all s, t, stop; otherwise, set $k = k + 1$ and return to Step 2.

5.2. Machine learning enhancements

To support and accelerate the APH process, machine learning methods are integrated as follows:

1. **Scenario Reduction**: Employ k-means clustering to reduce the number of scenarios while preserving key features of the uncertainty space. This approach reduces computational requirements and focuses on high-impact scenarios.
2. **Warm Start with Neural Networks**: Utilize a neural network to predict near-optimal initial solutions for $x_{s,t}^0$ based on scenario parameters, thereby decreasing the number of APH iterations required for convergence.
3. **RL for Adaptive Penalty Tuning**: RL is applied to tune γ in real-time, optimizing the APH algorithm's convergence trajectory and minimizing computational cost.

Before applying k-means clustering, the original scenario set was constructed through a staged process that combines historical datasets with stochastic projections. Specifically, hourly demand and renewable generation time series (wind, solar, tidal) were based on SONI records and project-level site data, while long-term drivers such as technology costs, discount rates, and CO_2 pricing were varied within published uncertainty ranges (see Table 4). Around these baselines, stochastic perturbations were introduced to create multiple plausible trajectories that capture both inter-annual variability and forward-looking policy or market developments. This ensures that the initial scenario pool represents a diverse space of plausible futures rather than a direct replication of historical trends. K-means clustering was then applied to this enriched set, reducing the computational burden while preserving representative variability across demand, resource, cost, and policy dimensions. Thus, historical data served only as parameter seeds, while robustness was ensured by embedding uncertainty bounds and stochastic variability before clustering, in line with long-term planning practices.

5.3. IGDT-FRM integration

To address the IGDT requirements within the IG-FRM-TSP framework, the solution method includes a robustness-focused post-optimization step:

1. **Post-Optimization Robustness Analysis**: Conduct a robustness evaluation of the obtained solution using the IGDT framework. This involves testing the sensitivity of the solution under various levels of uncertainty.
2. **Iterative Refinement Based on Robustness Level** α^*: If the robustness level α^* is unsatisfactory, update the C_{th} constraint parameters and re-run the APH algorithm with these adjusted constraints, further refining the solution's robustness.

5.4. Algorithm summary

The complete high-level solution methodology is outlined in Algorithm 1. This hybrid method creates a robust and flexible solution methodology tailored for the IG-FRM-TSP model. The combination of scenario reduction, adaptive penalties, and RL ensures computational efficiency and adaptability in handling complex uncertainties. For the complete detailed computational procedure, including specific implementation parameters and validation steps, refer to Algorithm 2 in the Appendix.

Algorithm 1 IG-FRM-TSP High-Level Solution Algorithm.

Stage 0: Perform data preparation and scenario reduction using k-means clustering
Stage 1: Initialize the APH algorithm with ML-predicted warm starts
while not converged **do**
    Solve bundled scenario subproblems in parallel
    Update averages and penalties for each bundle
    Adjust γ using RL
end while
Stage 3: Conduct IGDT-based robustness analysis to compute α^*
if α^* is unsatisfactory **then**
    Adjust C_{th}
    Return to Stage 1 with updated constraints
end if
Stage 4: Perform operational validation in DigSILENT
Stage 5: Return the final solution

6. Case studies and simulation results

The grid model in this study is developed in DIgSILENT PowerFactory, representing the 275 kV transmission network of Northern Ireland. To ensure accuracy and reliability, the model is validated against operational data provided by SONI [46], capturing key operational dynamics such as the frequent dispatch-down events in Northern Ireland caused by grid limitations and system stability requirements during periods of high renewable generation. Building on this, the base case snapshot was established and validated in DIgSILENT, and all final expansion scenarios obtained from the optimization framework were cross-checked to confirm that the resulting operational states are feasible under realistic network conditions. This process provides assurance that the capacity expansion results are not only cost-optimal in the optimization framework but also operationally valid in a commercial-grade simulation environment. While contingency and transient stability analyses are beyond the scope of this paper, they represent valuable directions for future work to complement the present operational validation. Following validation, the model is implemented in Python to perform the optimization and scenario analysis efficiently. This enables the assessment of multiple strategies for renewable integration, with particular emphasis on tidal energy's role in enhancing the generation mix and reducing dispatch-down events, thereby contributing to both grid stability and increased utilization of renewable resources.

6.1. Case studies

This section presents the evaluation of the proposed model under three scenarios reflecting different levels of decarbonization ambition for Northern Ireland. The scenarios are designed to assess the implications of tidal energy integration, renewable curtailment management, heating sector electrification, and energy storage deployment (battery and hydrogen) on overall system cost, CO_2 emissions, and system flexibility. The analysis utilizes 2022 operational data from SONI, with future projections informed by regional and national energy policy targets. The three scenarios modeled are as follows:

1. **Business-as-Usual (BAU):** This baseline scenario includes wind (both offshore and onshore), gas plants, solar photovoltaics, and battery energy storage systems, with no additional policy shifts or technological advancements beyond current trends.
2. **Advanced Renewable Integration (ARI):** This scenario examines the integration of tidal energy alongside increased storage deployment. Two tidal capacity levels are explored (100 MW and 260 MW), in conjunction with hydrogen production and storage via electrolysis. Battery storage remains available, and the SNSP

Table 1
Key assumptions of the simulated scenarios.

Feature	BAU	ARI-100 MW	ARI-260 MW	HED	HED (GasExit)
Tidal Source	No	100 MW	260 MW	260 MW	260 MW
Heating Electrification	No	No	No	Yes	Yes
Gas Plant	Retained	Retained	Retained	Retained	500 MW Decommissioned
SNSP Target	75 %	75 %	95 %	95 %	95 %
Battery Storage	Yes	Yes	Yes	Yes	Yes
Hydrogen Storage	No	Yes	Yes	Yes	Yes
Dispatch-down Penalty	No	Yes	Yes	Yes	Yes
CO_2 Emission Penalty	No	Yes	Yes	Yes	Yes
Tidal energy subsidies	No	No	No	No	Yes

constraint is progressively relaxed to 95 %, enabling a higher renewable share and lower curtailment.

3. **Heating Electrification Demand (HED):** The HED scenario builds on ARI by incorporating substantial electrification of the heating sector through heat pumps. It includes the full deployment of 260 MW of tidal energy, as well as hydrogen and battery storage. A sub-scenario is considered in which the 500 MW gas plant in Ballylumford is decommissioned.

The scenarios developed for this study incorporate progressively increasing SNSP limits to reflect advancements in grid stability measures and renewable integration targets. For the BAU scenario, the SNSP limit is set to 75 %, representing the current operational threshold in the Irish grid. In the ARI and HED scenarios, the SNSP limit is increased to 95 % for the year 2030 to align with national climate action goals. These staged SNSP adjustments provide insights into the grid's capability to accommodate higher renewable shares under different policy and technological advancements. Table 1 summarizes the assumptions across all scenarios.

Each scenario is evaluated using the IG-FRM-TSP methodology, which allows for a comprehensive techno-economic analysis of decarbonization strategies and renewable integration pathways tailored to Northern Ireland's energy goals. The sequential scenario design enables the isolation of individual technology impacts while building towards a power system capable of meeting ambitious net-zero targets. The case study for Northern Ireland draws on multiple datasets: high-resolution tidal velocity and power profiles from the X-Flow project at the Queen's University Belfast Tidal Test Site (Figs. 5 and 6), additional tidal site profiles generated by harmonic analysis [36], hourly wind and solar generation from SONI's 2022 operational dataset (Fig. 8), baseline and heating demand derived from SONI projections and gas-consumption conversions (Fig. 7), and the 275 kV transmission network model in DIgSILENT validated against SONI operational data (Fig. 4). Techno-economic parameters are summarized in Table 2, fuel and emission data in Table 3, uncertainty ranges and CO_2 price escalations in Table 4, and existing/candidate resources in Tables 5–7. These datasets anchor the Northern Ireland scenarios but also illustrate the type of information required for other jurisdictions

6.2. Simulation results

Fig. 4 illustrates the 270 kV transmission power grid model for Northern Ireland. The figure provides a representation of potential tidal energy integration points within the existing grid infrastructure. The capacities of sites vary, with the largest, T_2, having a confirmed capacity of 200 MW, T_5 at 30 MW, and T_1, T_3, and T_4 having undetermined capacities. These undetermined capacities are assumed to be 10 MW each in this study. The model represents a simplified transmission-level network, incorporating identified potential tidal and offshore wind sites, as detailed in Section 3, along with the Moyle HVDC interconnector to Scotland and AC interconnections to the Republic of Ireland. In this figure, the dashed lines represent candidate transmission connections, including subsea cables and overhead lines, considered for the integration of sites with capacities greater than 100 MW -specifically, W_1, T_2, and W_2. Sites with capacities up to 30 MW are assumed to be connected to the local distribution network, and thus their associated transmission costs are neglected. The high-capacity offshore sites (W_1, T_2, and W_2) are each assumed to require a 10 km subsea cable to the shore. Transmission routing assumptions are:

- T_2 to Coolkeeragh (60 km), Ballylumford (45 km), Kells (40 km)
- W_1 to Coolkeeragh (30 km)
- W_2 to Tandragee (45 km)

For W_1 and W_2, only one transmission connection option is considered, as alternative 275 kV substations are located relatively far and would incur significantly higher costs. For T_2, three different connection options are considered. These are geographically and economically comparable and offer opportunities for the grid to mitigate congestion and potentially replace existing gas power plants in Coolkeeragh and Ballylumford. The cost of the 275 kV transmission line is assumed to be 3 million per kilometer on average in this study.

Across all scenarios, the model incorporates:

- Dispatch-down costs to account for the curtailment of renewable resources
- CO_2 emission costs to internalize the environmental impact of energy production

The tidal generation profile is developed from data collected at site T_2, and scaled to represent a 200 MW tidal plant. Figs. 5 and 6 show the sample tidal velocity data from May and the corresponding scaled generation profile for a 200 MW capacity in 2030. For other sites lacking complete annual data, the model applies a predictive method from [36], leveraging harmonic analysis outputs to forecast tidal behavior over a 1-year period. This approach allows for systematic profiling of tidal energy potential across all candidate sites. The baseline power and heat demand considered in the model are shown in Fig. 7. The baseline power demand is applied directly in the BAU and ARI scenarios, where no additional heating load is considered. In the HED scenario, heating electrification is modeled by adding the corresponding heating demand on top of this baseline. The heat demand is derived from gas consumption data using a simple conversion approach; however, as only 20 % of this demand is incorporated into the model, the accuracy of the heat demand estimation is not a major concern in this study. The baseline scenario for onshore wind generation profiles is presented in Fig. 8.

Table 2 provides the input data for the model, including the costs and operational lifetimes of the various technologies considered. Table 3 presents the basic fuel and emission characteristics associated with each fuel type, detailing emission factors and primary energy content to support accurate calculation of environmental impacts and fuel-related costs. Most of the data presented in Table 2 are sourced from [47,48], providing a comprehensive basis for cost, lifespan, and operational parameters across various energy technologies. The values for tidal energy are specifically estimated based on projections from the

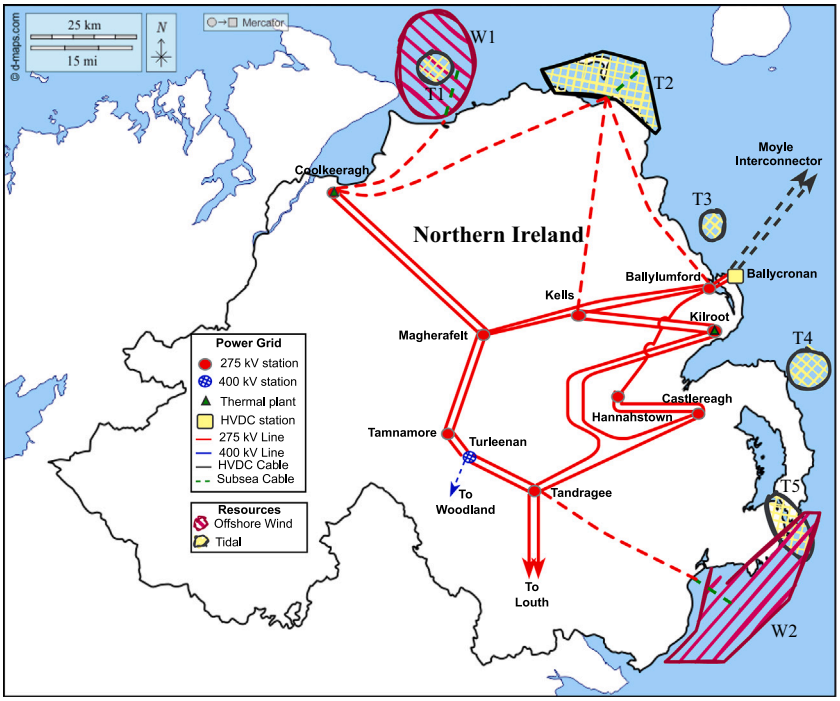

Fig. 4. Northern Ireland's power transmission grid.

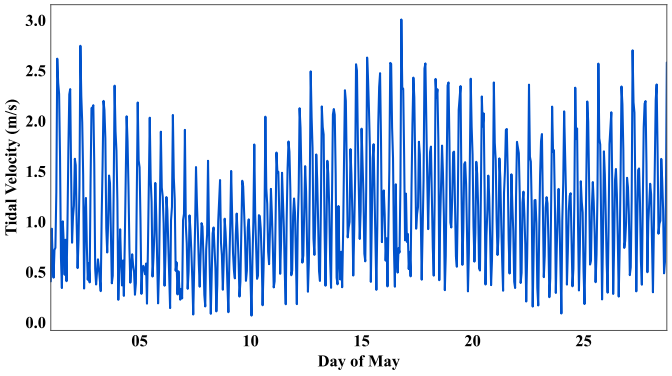

Fig. 5. Tidal velocity profile at site T2 for May 2014.

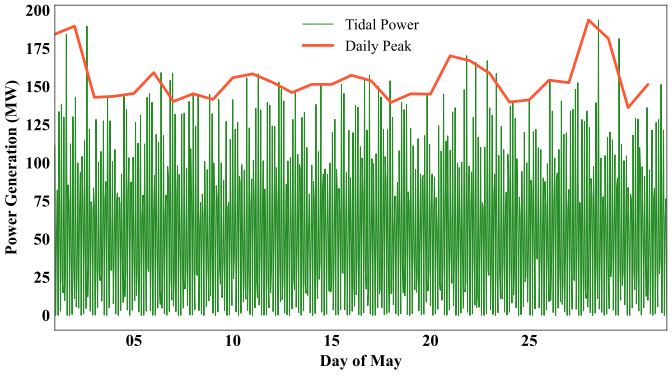

Fig. 6. Tidal power generation profile from measured velocity data.

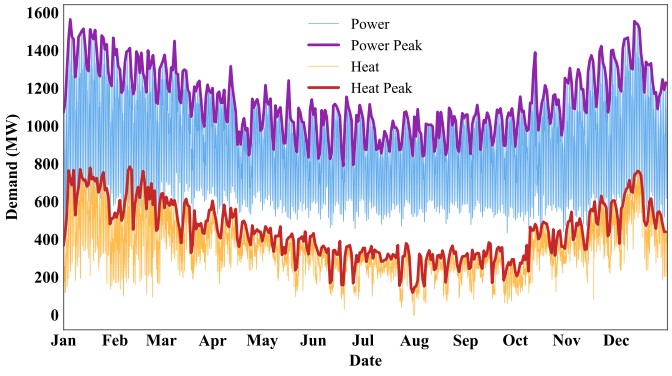

Fig. 7. Baseline demand Profiles for 2030.

X-Flow project, reflecting expected costs and performance characteristics for this technology under current development scenarios. Table 4 presents the uncertainty parameters and CO_2 cost escalation factors used in the mathematical model. These parameters account for variability in key factors such as demand, discount rates, technology costs, and renewable generation, which are essential for evaluating the system under different uncertainty scenarios. The uncertainty ranges are specified for each parameter, including demand uncertainty, discount rate uncertainty, technology cost uncertainty, and renewable generation uncertainty. Additionally, the CO_2 emissions are regulated through two thresholds: a low emission threshold of 0.5 Mtons and a high emission threshold of 1.0 Mtons. The CO_2 cost is escalated using multiplicative factors of 1.25 when emissions are between these thresholds and 1.50 when emissions exceed the high threshold. These escalation factors ensure that the model incorporates financial impacts tied to emissions, supporting the system's transition toward decarbonization. The base discount rate used for the financial analysis is set at 0.04, reflecting standard economic assumptions for long-term investment decisions.

The main generation and storage configurations used in the simulations are provided in Tables 5–7. Table 5 summarizes the existing generation sources, while Tables 6 and 7 present the candidate generation and storage capacities considered across the BAU, ARI, HED, and

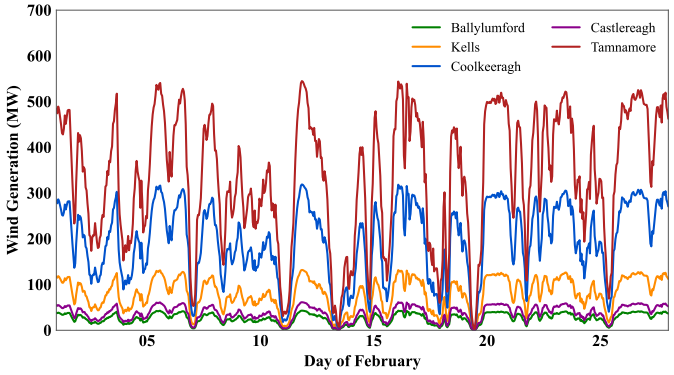

Fig. 8. Hourly wind generation profile at key sites, February 2030.

Table 2
Key input values for various technologies in 2030.

Technology	Cost (M€/MW)	Life (Year)	Fixed O&M (% of Cost)
CCGT	0.95	35	2.5
Onshore Wind	1.34	25	2.5
Offshore Wind	2.52	25	3.0
Solar	0.86	25	1.5
Fuel Cell	0.80	25	2.5
Electrolysis	0.60	25	3.0
Battery Storage	1.12	20	1.0
H_2 Storage	1.80	40	1.5
Tidal	3.50	25	3.0

Table 3
Fuel costs and emissions.

Fuel	Cost ($€/MW_{th}$)	Emission (tCO_2/MW_{th})
Natural Gas	57	0.37
BESS charge	50	–
Hydrogen	100	0.05

Table 4
Uncertainty parameters and CO_2 cost escalation factors.

Parameter	Value/Range
c^{DD}	100 €/tonne
C^{CO_2}	100 €/MWh
β_{demand}	[−0.1, 0.1]
$\beta_{\text{discount rate}}$	[−0.15, 0.15]
$\beta_{\text{technology cost}}$	[−0.2, 0.2]
$\beta_{\text{renewable}}$	[−0.15, 0.15]
cap_{low}	0.5
cap_{high}	1.0
δ_1	1.25
δ_2	1.50

Table 5
Existing generation sources.

No	Bus	Technology	Capacity (MW)
1	Ballylumford	CCGT	635
2	Coolkeeragh	CCGT	425
3	Tamnamore	PV	72
4	Kells	PV	72
5	Ballylumford	Onshore wind	53
6	Kells	Onshore wind	164
7	Coolkeeragh	Onshore wind	396
8	Castlereagh	Onshore wind	16
9	Tamnamore	Onshore wind	677

Table 6
Candidate generation and storage sources for BAU/ARI-100 MW/HED scenarios.

No	Bus	Technology	Capacity (MW)
1	Kilroot	CCGT	500
2	Bally/Kells/Cool	Tidal	100 and 260
3	Ballylumford	Offshore wind	200
4	Coolkeeragh	Offshore wind	200
5	Kells	Onshore wind	200
6	Castlereagh	Onshore wind	200
7	Tamnamore	Onshore wind	200
8	Kells	Solar PV	100
9	Tandragee	Solar PV	100
10	Kells	BESS	50
11	Coolkeeragh	BESS	100
12	Ballylumford	BESS	50
13	Tamnamore	BESS	100
14	Ballylumford	HES	100
15	Castlereagh	HES	50
16	Tandragee	HES	50
17	Coolkeeragh	HES	100

Table 7
Candidate generation and storage sources for the HED-GasExit scenario.

No	Bus	Technology	Capacity (MW)
1	Kilroot	CCGT	0
2	Bally/Kells/Cool	Tidal	360
3	Ballylumford	Offshore wind	300
4	Coolkeeragh	Offshore wind	300
5	Kells	Onshore wind	200
6	Castlereagh	Onshore wind	200
7	Tamnamore	Onshore wind	200
8	Kells	Solar PV	200
9	Tandragee	Solar PV	200
10	Kells	BESS	100
11	Coolkeeragh	BESS	100
12	Ballylumford	BESS	100
13	Tamnamore	BESS	100
14	Ballylumford	HES	100
15	Castlereagh	HES	100
16	Tandragee	HES	100
17	Coolkeeragh	HES	100

HED-GasExit scenarios. These configurations form the basis for the system expansion and operational analyses. The accuracy of the optimized generation in the output results is considered to be within a 5 MW margin. Although the model is based on real values, the output generation values have been rounded for simplicity and clarity. In the BAU scenario, the 500 MW Combined Cycle Gas Turbine (CCGT) at Kilroot is included, reflecting the real plan for its addition to the grid. However, as this paper focuses on evaluating net-zero target plans, the Kilroot CCGT is not considered in the HED-GasExit scenario. The Moyle HVDC interconnector, with a capacity of 500 MW, facilitates the transfer of power between the Northern Ireland and Great Britain electricity markets. For the purpose of simplifying the model, market trading is not explicitly modeled. Instead, an average cost of 300 €/MWh, reflecting market-related costs, is applied to power imports into the Northern Ireland grid.

The comprehensive outcomes of the proposed IG-FRM-TSP model, applied across the BAU, ARI, and HED scenarios outlined in Table 1, are presented in the continuation of this section. The results emphasize the techno-economic trade-offs involved in increasing renewable penetration, enhancing storage deployment, and integrating tidal energy under high SNSP conditions. In particular, the role of tidal energy as a complementary source to wind, its interaction with energy storage, and its potential to reduce system emissions is explored. Table 8 compares key system-level metrics across all scenarios, including total annualized cost, CO_2 emissions, renewable energy share, and curtailment rates.

Table 8
Comparative energy system metrics across scenarios.

Metric	BAU	ARI–100 MW	ARI–260 MW	HED	HED–GasExit
Total Annualized Cost (M€)	356.1	571.2	620.4	806.7	949.3
CO_2 Emissions (Mt)	1.069	0.292	0.218	0.365	0.268
Renewable Share (%)	37.5	59.2	61.8	62.5	65.2
SNSP (%)	38.8	75.0	85.6	87.1	88.47
Curtailment Rate (%)	6.8	2.6	1.9	4.8	10.6

The model confirms that progressive electrification combined with high renewable integration, especially tidal energy and storage, enables a significant cost-effective reduction in emissions.

The scenario analysis demonstrates that Northern Ireland's transition to a low-carbon energy system hinges on the interplay between renewable technologies, storage, and demand-side flexibility. The BAU scenario, with its reliance on gas-fired generation (500 MW CCGT) and limited renewables (37.5 % share), yields the lowest annualized cost (356.1 M€) but fails to meet decarbonization targets (1.069 $MtCO_2$).

To assess the sensitivity of wind-dominated systems, offshore wind data were projected using historical onshore wind profiles, scaled by 10 % to reflect higher capacity factors. In ARI-100 MW, this adjustment prioritizes offshore wind (330 MW) over tidal (100 MW) due to its cost competitiveness. However, when the scaling factor is increased to 15 %, offshore wind's economic advantage grows, further reducing its curtailment. Notably, introducing a 20 % subsidy for tidal energy reverses this dynamic: even with a 15 % wind profile uplift, tidal becomes the preferred dispatch priority, highlighting the impact of policy incentives on technology deployment. In the ARI–100 MW scenario, the SNSP limit is reached based on the output results, indicating that the integration of renewable energy sources is near the threshold of what the system can handle without risking grid stability.

The ARI-260 MW scenario, featuring 260 MW of tidal capacity paired with hydrogen storage (200 MW HES), achieves an 80 % reduction in emissions (0.218 Mt$CO2$) compared to BAU, despite a 74 % cost increase (620.4 M€). Although tidal energy's semi-diurnal generation profile does not consistently align with peak demand periods due to natural timing shifts, its predictable output helps reduce curtailment to 1.9 % (vs. 6.8 % in BAU) and displace gas-fired generation. The €100/MWh dispatch-down penalty and €100/tonne CO_2 penalty applied in the ARI and HED scenarios further enhance the economic competitiveness of tidal power by penalizing fossil-fueled flexibility and incentivizing firm renewable dispatch. To account for offshore wind's higher capacity factors, all scenarios apply a 10 % uplift to historical onshore wind profiles when modeling offshore wind generation.

Under this baseline adjustment, tidal energy consistently maintains dispatch priority over offshore wind despite its 20 % higher capital cost. This counterintuitive result stems from tidal generation's inherent advantages: its predictable semi-diurnal cycle provides a reliable and firm capacity that helps minimize dispatch-down penalties and reduces reliance on costly peaking units during periods of system stress. The model quantifies these benefits through reduced curtailment rates and lower total system costs when accounting for the €100/MWh dispatch-down and €100/tCO_2 penalties.

However, this equilibrium proves sensitive to wind generation characteristics. When the offshore wind profile scaling increases to 15 %, the combined effect of higher capacity factors and improved generation timing erodes tidal's economic advantage. The enhanced wind availability during traditional off-peak periods, coupled with tidal's persistent cost premium, triggers a priority inversion where offshore wind becomes the preferred dispatch option. This transition occurs even while maintaining all penalty structures, demonstrating how modest improvements in variable renewable productivity can fundamentally alter technology stacking decisions.

The balance between these generation sources remains highly responsive to policy interventions. Introducing a 20 % tidal subsidy effectively counters the 15 % wind profile enhancement, maintaining tidal's dispatch priority through targeted economic support. This demonstrates the crucial role of policy design in shaping technology adoption pathways, particularly for complementary renewable portfolios. Such mechanisms can preserve system diversity even when natural resource characteristics might otherwise favor a single dominant technology, ensuring the retention of tidal energy's grid-stabilizing benefits while still accommodating improvements in wind generation potential. Table 9 presents the installed capacity of different technologies across various scenarios. Relative to the modeled peak demand of 1510 MW in baseline scenarios, the installed storage power corresponds to 0 % (BAU), 19.87 % (ARI-100), and 20.53 % (ARI-260). In heating electrification scenarios, where peak demand increases to 1822 MW, storage capacities are 21.96 % (HED) and 32.94 % (HED-GasExit).

Table 9
Comparative performance of offshore wind and tidal energy across scenarios.

Metric	BAU	ARI-100	ARI-260	HED	HED-GasExit
CCGT (MW)	500	0	0	0	0
Offshore Wind (MW)	0	330	300	400	600
Onshore Wind (MW)	0	140	65	100	200
PV (MW)	0	0	0	0	200
Tidal (MW)	0	100	260	260	360
BESS (MW)	0	0	110	100	300
HES (MW)	0	300	200	300	300

The HED scenario examines the impacts on the power system when 20 % of the heat demand in Fig. 7 transitions to electric heat pumps. This partial electrification drives an average 16.5 % increase in annual electricity consumption compared to the BAU and ARI scenarios, yet the system successfully accommodates this additional demand while reducing emissions to 0.365 $MtCO_2$ - a 66 % reduction from BAU. This achievement comes from the coordinated operation of 260 MW tidal generation, 400 MW offshore wind, and 400 MW energy storage, which collectively maintain the reliability of the system while limiting the renewable curtailment to 4.8 %.

The more ambitious HED-GasExit scenario demonstrates the system's breaking points when pushing decarbonization further under the same 20 % heat electrification assumption. Removing the 446 MW Ballylumford gas plant while maintaining identical electrification levels exposes critical infrastructure gaps, manifested in a soaring curtailment to 10.6 % and a cost increase to 949.3 M€. These results reveal the hidden dependencies of current electrification pathways on fossil-based flexibility, even at modest heat pump penetration rates.

The quantified results demonstrate that the modeled storage portfolio (300 MW HES + 300 MW BESS) becomes insufficient to maintain system reliability when simultaneously implementing 20 % heat electrification and complete gas plant retirement, as evidenced by the 10.6 % curtailment rate and 949.3 M€ cost in HED-GasExit. This analysis provides concrete evidence that heat electrification strategies must be co-optimized with capacity expansion plans, particularly for systems targeting complete fossil phase-out.

Although the simulation covers the full year of 2030 across all scenarios, to avoid lengthening the paper, detailed results are presented for the HED-GasExit scenario, which represents the most complex and challenging case. The January profiles are extracted to provide a clearer analysis

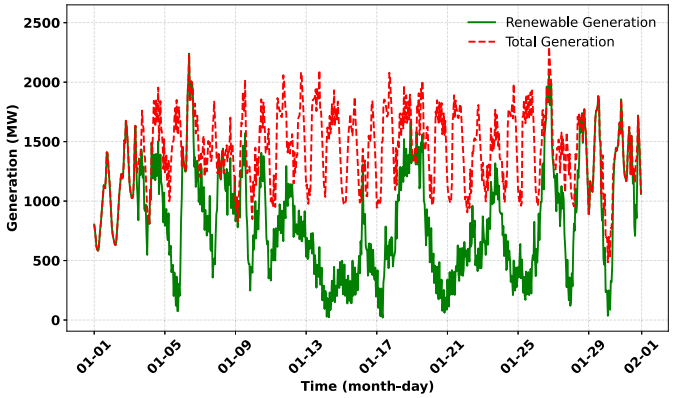

Fig. 9. Total and renewable generation profiles in the HED-GasExit scenario.

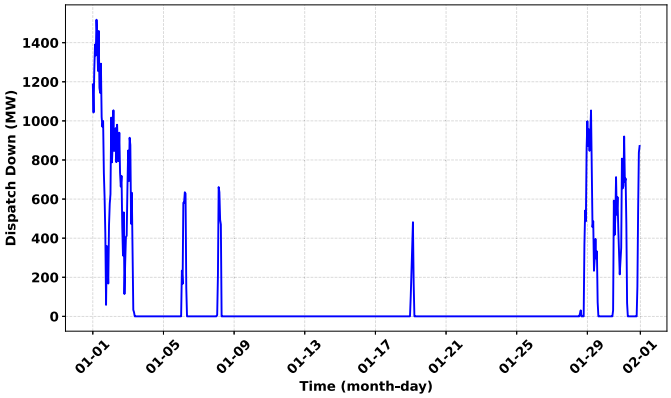

Fig. 11. Hourly dispatch down in the HED-GasExit scenario.

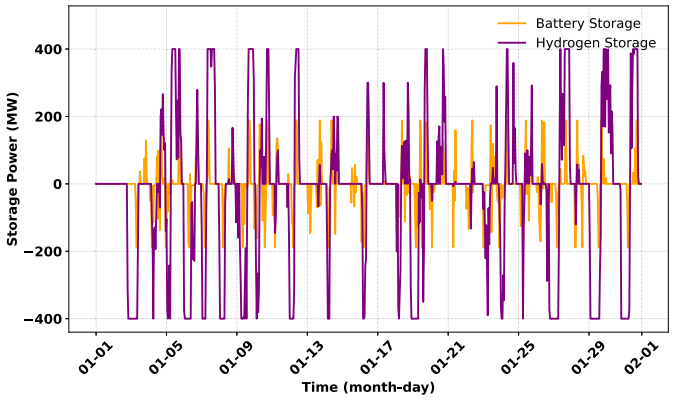

Fig. 10. Storage charge and discharge profile in the HED-GasExit scenario.

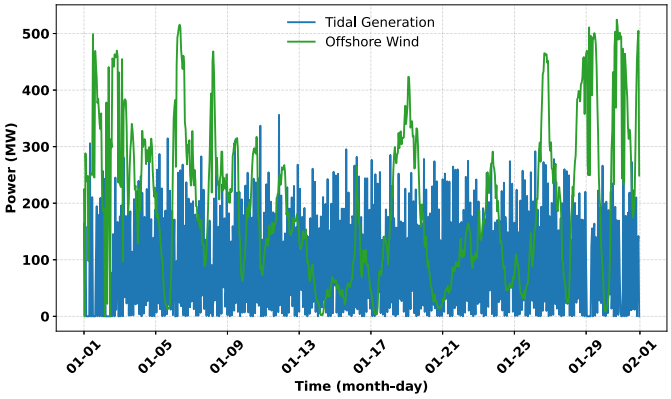

Fig. 12. Tidal and offshore wind generation profiles in the HED-GasExit scenario.

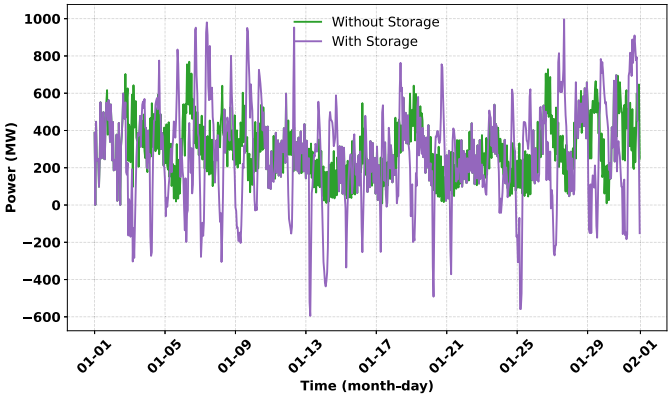

Fig. 13. Tidal and offshore wind generation with and without energy storage in the HED-GasExit scenario.

of system dynamics. The simulated operation for January 2030 highlights critical interdependencies between generation profiles, storage behavior, and system constraints. As shown in Fig. 9, a consistent diurnal pattern emerges, with renewable generation (primarily wind and tidal) peaking at 2200 MW during high-wind periods. Dispatchable sources supply the remaining demand, particularly during the evening ramp between 17:00 and 21:00 when renewable output typically declines. Fig. 10 illustrates the complementary operation of storage technologies over the month. Battery storage provides rapid, sub-hourly cycling to manage short-term imbalances, while hydrogen storage engages in multi-day energy shifting, particularly during extended low-wind periods around mid-month. The net discharge cycle aligns closely with the evening demand peak, offsetting approximately 300 MW of conventional generation requirements. System constraints become apparent in Fig. 11, where curtailment events peak at 1450 MW during high-wind, low-demand periods. In HED-GasExit, storage operation offsets about 300 MW (16.5 % of peak) of conventional generation during evening peaks. These events occur predominantly in the 2nd week of January, when renewable generation exceeds 90 % of the total system output. The dispatch-down profile exhibits an inverse correlation with storage state-of-charge levels, highlighting opportunities for optimized storage bidding strategies.

Several key operational insights emerge from the January simulation. The 20 % level of heat electrification visibly intensifies the evening demand ramp, necessitating fossil backup under current conditions. Storage systems demonstrate effective load-shifting capability, successfully transferring 18 %–22 % of daily renewable generation to peak demand periods. Although the existing infrastructure appears sufficient to accommodate January's conditions, stress points emerge during extended low-renewable periods, indicating areas for potential reinforcement. Overall, these outputs quantitatively validate the scenario assumptions while revealing specific opportunities for improvement in storage sizing and renewable-storage coordination strategies.

Figs. 12 and 13 present the renewable generation and system output profiles for January, considering installed capacities of 600 MW offshore wind and 360 MW tidal energy. Although this configuration does not yet reflect current real-world deployments, it serves as a critical case study for exploring the dynamics and policy requirements associated with large-scale marine renewable integration coupled with energy

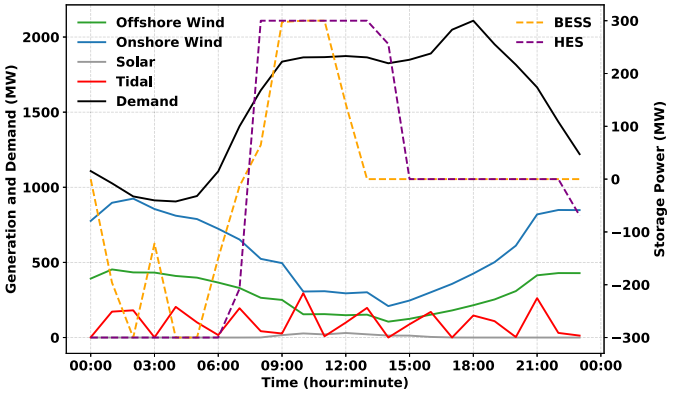

Fig. 14. Typical-day generation and storage time-series (mid-February) for the HED-GasExit scenario.

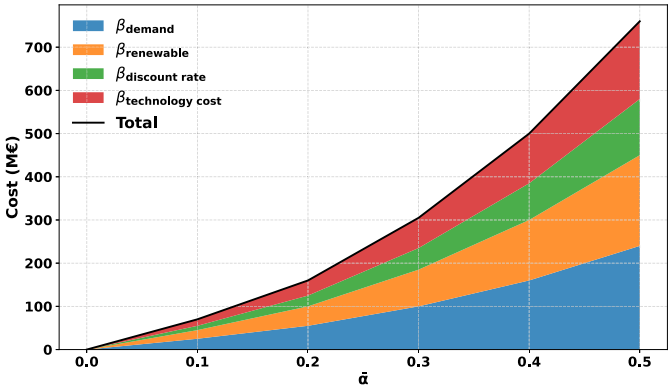

Fig. 15. Cost decomposition under deep uncertainty for increasing $\bar{\alpha}$.

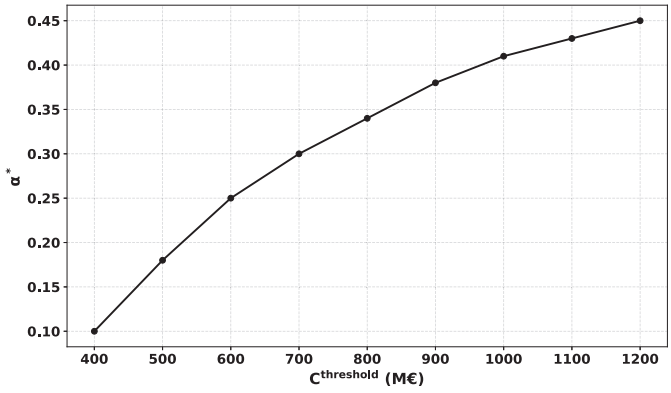

Fig. 16. System robustness as a function of cost tolerance.

storage systems. Analysis of the generation profiles reveals the distinct operational characteristics of the two marine sources. Tidal generation exhibits a highly predictable semi-diurnal pattern, with outputs varying between approximately 50 MW and 200 MW over daily cycles. The predictability of tidal energy offers a valuable firm capacity contribution, although its maximum output remains lower than that of offshore wind. In contrast, offshore wind generation is characterized by considerable volatility, with output frequently oscillating between near-zero and up to the full installed capacity of 600 MW, driven by atmospheric conditions. The combined marine generation profile thus benefits from the complementary behavior of tidal energy, which partially offsets the intermittency of offshore wind; however, substantial fluctuations persist at the system level.

The aggregated system output, shown in Fig. 13, further highlights the role of energy storage. Without storage, the system output mirrors the variability of renewable generation, leading to periods of surplus and deficit relative to demand. When storage is incorporated, the system output profile becomes markedly more dynamic, with fluctuations ranging from approximately -600 MW to $+1000$ MW. Notably, rather than purely smoothing renewable generation, storage assets actively participate in system balancing: charging during periods of excess and discharging during shortfalls. Consequently, storage operations introduce additional dynamics into the system output, reflecting their role not only in mitigating renewable variability but also in meeting demand requirements more flexibly. This behavior carries significant implications for policy and system design.

Fig. 14 presents a representative mid-February day, illustrating the intra-day interaction among tidal, offshore wind, onshore wind, and solar generation, together with system demand and storage operation. This higher-resolution view highlights the distinctive role of tidal generation and its coordination with storage. Tidal output follows a predictable semi-diurnal cycle with two clear peaks per day, in contrast to the larger and less regular fluctuations of offshore wind. Although its magnitude is lower—typically in the tens to hundreds of megawatts—tidal generation provides a highly reliable and forecastable contribution. Its regular peaks supply a consistent marine baseline that reduces short-term reliance on thermal units, while their predictability enables more efficient scheduling of BESS and HES, improving system balance and reducing renewable curtailment. The inherent predictability of tidal energy offers a strategic advantage for system reliability and should be reflected in capacity market design and dispatch planning. Integrating tidal with offshore wind can substantially raise renewable penetration but also requires investment in flexible, dispatchable storage systems. Overall, the results underscore the complementary value of tidal generation and the necessity of co-developing offshore renewables and storage infrastructure to achieve a stable, high-renewable power system for Northern Ireland.

In addition to scenario-based results, it is essential to demonstrate how the IGDT framework explicitly handles deep uncertainty. To this end, Figs. 15 and 16 are introduced to quantify the role of uncertainty sets and robustness measures in long-term planning under disruptive future conditions. These figures complement the stochastic analyses presented earlier by offering a non-probabilistic evaluation of system resilience. Fig. 15 illustrates how the expansion cost evolves under deep uncertainty when the uncertainty horizon $\bar{\alpha}$ increases. The four components correspond to the parameter-specific deviation bounds β_{demand}, $\beta_{\text{renewable}}$, $\beta_{\text{discount rate}}$, and $\beta_{\text{technology cost}}$, as defined in Table 4. As $\bar{\alpha}$ grows, the uncertainty set $U(\bar{\alpha})$ expands, and the worst-case system cost rises accordingly. Demand and renewable uncertainty exert the largest influence, while interest rate and policy deviations contribute more moderately. The total line confirms that the model explicitly captures the non-probabilistic nature of IGDT by evaluating the most adverse realization within $U(\bar{\alpha})$.

Fig. 16 presents the IGDT robustness function, showing the maximum achievable robustness horizon α^* as a function of the acceptable cost threshold C_{th}. For a relatively tight cost tolerance, only a small α^* is sustainable. As the threshold relaxes, α^* increases, meaning the system can withstand broader deviations in β_{demand}, $\beta_{\text{renewable}}$, $\beta_{\text{discount rate}}$, and $\beta_{\text{technology cost}}$ without violating the cost constraint. The curve exhibits diminishing returns: beyond a certain point, large cost relaxations yield only marginal gains in robustness. This result demonstrates how IGDT quantifies robustness under deep uncertainty and complements the stochastic layer of the model.

7. Conclusion

This study demonstrates tidal energy's pivotal role in Northern Ireland's decarbonization strategy when integrated with offshore wind

and hybrid storage systems. Scenario analyses using the novel IG-FRM-TSP framework reveal that 260 MW tidal capacity, 400 MW offshore wind, and 400 MW storage achieve a 66 % CO_2 reduction in the HED scenario compared to BAU. The ARI-260 MW scenario further reduces emissions by 80 % (0.218 $MtCO_2$), leveraging tidal predictability to align generation with demand peaks, minimizing curtailment to 1.9 %-a fivefold improvement over BAU. HES proves critical for multi-day energy shifting, offsetting 300 MW of conventional generation during demand surges. However, retiring the 500 MW Ballylumford CCGT plant without adequate storage scaling (HED-GasExit scenario) elevates curtailment to 10.6 %, exposing residual fossil dependency. While storage mitigates short-term imbalances, week-long deficits necessitate larger HES reserves (>300 MW). The IG-FRM-TSP framework, highlights policy-sensitive equilibria: tidal dispatch priority persists under baseline assumptions but shifts to offshore wind with a 15 % capacity scaling, unless a 20 % tidal subsidy rebalances economics. A key limitation is the static analysis of high-renewable scenarios, warranting future time-domain stability studies to assess transient grid dynamics. Northern Ireland's net-zero pathway by 2030 requires strategic tidal-hydrogen co-deployment, policy incentives for technology diversity, and grid resilience upgrades. This work provides a replicable model for coastal regions, emphasizing that tidal predictability and storage responsiveness—not just capacity—dictate decarbonization efficacy.

CRediT authorship contribution statement

Vahid Sabzpoosh Saravi: Writing – original draft, Validation, Software, Methodology, Investigation, Formal analysis, Data curation, Conceptualization. **Xueqin Liu:** Writing – review & editing, Supervision, Methodology, Investigation, Funding acquisition, Data curation, Conceptualization. **Carwyn Frost:** Writing – review & editing, Supervision, Funding acquisition, Data curation.

Declaration of competing interest

The authors declare the following financial interests/personal relationships which may be considered as potential competing interests:

Vahid Sabzpoosh Saravi, Xueqin Liu, Carwyn Frost report that financial support was provided by the Northern Ireland Department for the Economy. If there are other authors, they declare that they have no known competing financial interests or personal relationships that could have appeared to influence the work reported in this paper.

Acknowledgement

The authors gratefully acknowledge support from the Green Innovation Challenge Fund, led by the Centre for Advanced Sustainable Energy (CASE) as delivery partner for the Department for the Economy, Northern Ireland, under the project titled 'X-flow'. This support was instrumental in enabling the research and development presented in this paper.

Appendix A. Detailed solution algorithm and validation procedure of the IG–FRM–TSP model

This appendix presents the complete computational sequence used to solve the IG–FRM–TSP model. It expands upon Algorithm 1 in the main text and provides a detailed description of (i) the optimization steps, (ii) the IGDT-based reliability assessment, and (iii) the post-optimization validation performed in DIgSILENT. Solver settings, scenario data, and parameter values are consistent with those reported in Tables 2–4. The optimization model is formulated as a MILP problem and implemented in a Python environment. Convergence tolerances of $\varepsilon_{\text{APH}} = 10^{-4}$ and $\varepsilon_{\text{IGDT}} = 10^{-3}$ are adopted. The algorithm integrates stochastic optimization through the APH method, an IGDT-based robustness evaluation, and a post-optimization reliability validation using the DIgSILENT power-flow environment. This integrated framework ensures that the optimal solutions obtained by the IG–FRM–TSP model are both economically sound and operationally feasible.

Algorithm 2 Solution algorithm for the IG–FRM–TSP model.

Require: Hourly renewable and demand data, techno–economic parameters, scenario set $\mathcal{S}$, solver tolerances $(\varepsilon_{\text{APH}}, \varepsilon_{\text{IGDT}})$, and cost threshold C_{th}.

Stage 0: Data preparation
Import hourly renewable generation time series and system demand.
Generate perturbed scenarios according to uncertainty bounds β_i and construct $\mathcal{S}$.
Apply k–means clustering to reduce temporal resolution.
Stage 1: Initialization
Set iteration counter $k = 0$.
Initialize decision variables $x^0_{s,t}$ and $y^0_{s,t}$ (capacity and dispatch), and penalty factor $\gamma = \gamma_0$.
Initialize bundle weights $w_{s,t} = 0$ and supply warm start using neural network predictor when available.
Stage 2: APH loop
while not converged **do**
    Partition $\mathcal{S}$ into parallel bundles and solve each bundle subproblem with current γ and $w_{s,t}$.
    Aggregate scenario averages $\bar{x}^{k+1}_t$ and update penalties: $w_{s,t} \leftarrow w_{s,t} + \gamma(x^{k+1}_{s,t} - \bar{x}^{k+1}_t)$.
    Adapt γ using the RL rule.
    if $\max_{s,t} \|x^{k+1}_{s,t} - \bar{x}^{k+1}_t\| < \varepsilon_{\text{APH}}$ **then**
        break
    else
        $k \leftarrow k + 1$
    end if
end while
Stage 3: IGDT reliability assessment
Evaluate robustness parameter α^* by binary search on $\bar{\alpha} \in [0, \alpha_{\max}]$:
for each test value $\bar{\alpha}$ **do**
    Construct uncertainty set $\mathcal{U}(\bar{\alpha})$ using scaled deviations $\beta_i \bar{\alpha}$.
    For worst-case samples $\xi \in \mathcal{U}(\bar{\alpha})$, compute total cost $C_{\text{tot}}(\xi)$ and feasibility of (x, y).
    if $C_{\text{tot}}(\xi) \le C_{\text{th}}$ for all $\xi \in \mathcal{U}(\bar{\alpha})$ **then**
        $\alpha^* \leftarrow \bar{\alpha}$ (feasible)
    else
        infeasible; reduce $\bar{\alpha}$.
    end if
    if $|\Delta\bar{\alpha}| < \varepsilon_{\text{IGDT}}$ **then break**
    end if
end for
Stage 4: DIgSILENT post-optimization validation
Map optimized dispatch and network capacities to the corresponding DIgSILENT model.
Run steady-state AC power flow and verify: (i) bus voltage limits, (ii) branch loading, and (iii) SNSP.
if violations ≤ tolerance **then**
    Accept solution.
else
    Record violations and update network; return to Stage 2.
end if
Stage 5: Output and scenario comparison
Export final capacities x^*, dispatch y^* and robustness index α^*.
Compare results across scenarios in terms of cost, renewable penetration, and curtailment.

Data availability

The data used are publicly available, and references are provided in the manuscript.

References

[1] Department for the Economy, Northern Ireland. Electricity consumption and renewable generation in Northern Ireland: April 2024 to March 2025, Tech. rep., Department for the Economy, Northern Ireland, statistical report confirming statutory target of at least 80 % renewable electricity by 2030 under the Climate Change Act (Northern Ireland) 2022 (June 2025). https://www.nisra.gov.uk/news/43-electricity-consumption-was-generated-renewable-sources-located-northern-ireland.

[2] International Renewable Energy Agency. Global Offshore wind report 2022, Tech. rep. Abu Dhabi: IRENA; 2022.

[3] Connor Jordan DD. Combining shallow-water and analytical wake models for tidal array micro-siting. J Ocean Eng March Energy 2022;8:193–215. https://doi.org/10.1007/s40722-022-00225-2

[4] Khare V, Bhuiyan M. Tidal energy-path towards sustainable energy: a technical review. Clean Energy Syst 2022;3:16. https://doi.org/10.1016/j.cles.2022.100041

[5] Garrett C. Tidal power's limits. Phys Today 2024;77(3):11. https://doi.org/10.1063/pt.bjfi.zbdn

[6] Coles D, Angeloudis A, Goss Z, Miles J. Tidal stream VS. wind energy: the value of cyclic power when combined with short-term storage in hybrid systems. Energies 2021;14(4). https://doi.org/10.3390/en14041106

[7] Segura E, Morales R, Somolinos J, Lopez A. Techno-economic challenges of tidal energy conversion systems: current status and trends. Renew Sustain Energy Rev 2017;77:536–50.

[8] Roberts A, Thomas B, Sewell P, Khan Z, Balmain S, Gillman J. Current tidal power technologies and their suitability for applications in coastal and marine areas. J Ocean Eng March Energy 2016;2:227–45. https://doi.org/10.1007/s40722-016-0044-8

[9] Noble DR, Grattan K, Jeffrey H. Assessing the costs of commercialising tidal energy in the UK. Energies 2024;17(9). https://doi.org/10.3390/en17092085. https://www.mdpi.com/1996-1073/17/9/2085.

[10] Coles D, Wray B, Stevens R, Crawford S, Pennock S, Miles J. Impacts of tidal stream power on energy system security: an Isle of Wight case study. Appl Energy 2023;334:120686. https://doi.org/10.1016/j.apenergy.2023.120686

[11] University of Edinburgh. 2023 annual review of UK marine energy sector, Technical report, University of Edinburgh, 2023. Available at: https://marineenergycouncil.co.uk/news/2023-a-turning-point-for-uk-marine-energy-according-to-new-report.

[12] Zhang Y, et al. Hydrogen as an energy vector in renewable energy systems. Int J Hydrogen Energy 2022;47:101–12. https://doi.org/10.1016/j.ijhydene.2021.09.123

[13] Vorushylo I, Keatley P, Shah N, Green R, Hewitt N. How heat pumps and thermal energy storage can be used to manage wind power: a study of Ireland. Energy 2018;157:539–49. https://doi.org/10.1016/j.energy.2018.03.001

[14] European Marine Energy Centre. Flow batteries to combine with tidal power to produce world's first continuous green hydrogen, Tech. rep., EMEC; 2021. https://www.emec.org.uk/flow-batteries-combine-with-tidal-power-to-produce-green-hydrogen.

[15] Liu Y, et al. Energy storage solutions for renewable energy systems. Renew Sustain Energy Rev 2023;158:112–23. https://doi.org/10.1016/j.rser.2022.112123

[16] Ullah F, Zhang X, Khan M, Mastoi MS, Munir HM, Flah A, Said Y. A comprehensive review of wind power integration and energy storage technologies for modern grid frequency regulation. Heliyon 2024;10(9):e30466. https://doi.org/10.1016/j.heliyon.2024.e30466

[17] Osman P, Hayward JA, Penesis I, Marsh P, Hemer MA, Griffin D, Sayeef S, Nader J-R, Cossu R, Grinham A, Rosebrock U, Herzfeld M. Dispatchability, energy security, and reduced capital cost in tidal-wind and tidal-solar energy farms. Energies 2021;14(24). https://doi.org/10.3390/en14248504

[18] Peerzada A, Hanif S, Tarekegne B, Baldwin D, Bhattacharya S. On the impact of tidal generation and energy storage integration in PV-rich electric distribution systems. Appl Energy 2024;357:122466. https://doi.org/10.1016/j.apenergy.2023.122466

[19] Gaffney F, Deane JP, Drayton G, Glynn J, Gallachóir BÓ. Comparing negative emissions and high renewable scenarios for the European power system. BMC Energy 2020;2(1):1–13. https://doi.org/10.1186/s42500-020-00013-4

[20] Coker P, Barlow J, Cockerill T, Shipworth D. Measuring significant variability characteristics: an assessment of three UK renewables. Renew Energy 2020;156:1361–70. https://doi.org/10.1016/j.renene.2019.10.131

[21] Argyrou MC, Christodoulides P, Kalogirou SA. Energy storage for electricity generation and related processes: technologies appraisal and grid scale applications. Renew Sustain Energy Rev 2018;94:804–21. https://doi.org/10.1016/j.rser.2018.06.044

[22] SONI. Northern Ireland constraints report 2023, Tech. rep., SONI Ltd; 2023. https://cms.soni.ltd.uk/sites/default/files/media/documents/20231012b_NI-Constraints_2023_Final-Report_v1.pdf [Accessed 22 Dec. 2024].

[23] Wang Y, et al. Economic assessment of tidal energy technologies. Renew Energy 2021;164:150–62. https://doi.org/10.1016/j.renene.2020.10.024

[24] Coles D, Angeloudis A, Greaves D, Hastie G, Lewis M, Mackie L, McNaughton J, Miles J, Neill S, Piggott M, Risch D, Scott B, Sparling C, Stallard T, Thies P, Walker S, White D, Willden R, Williamson B. A review of the UK and British channel Islands practical tidal stream energy resource. Proc R Soc A Math Phys Eng Sci 2021;477(2255):20210469.

[25] Bianchi M, Arnal AJ, Astorkiza-Andres M, Clavell-Diaz J, Marques A, Isasa-Sarralde M. Life cycle and economic assessment of tidal energy farms in early design phases: application to a second-generation tidal device. Heliyon 2024;10(12):e32515. https://doi.org/10.1016/j.heliyon.2024.e32515

[26] International Energy Agency. Global hydrogen Review 2023, Tech. rep., International Energy Agency (IEA); 2023. https://www.iea.org/reports/global-hydrogen-review-2023.

[27] Benghanem M, Mellit A, Almohamadi H, Haddad S, Chettibi N, Alanazi AM, Dasalla D, Alzahrani A. Hydrogen production methods based on solar and wind energy: a review. Energies 2023;16(2). https://doi.org/10.3390/en16020757

[28] Pourakbari-Kasmaei M, Asensio M, Lehtonen M, Contreras J. Trilateral planning model for integrated community energy systems and pv-based prosumers—a bilevel stochastic programming approach. IEEE Trans Power Syst 2019;35(1):346–61. https://doi.org/10.1109/TPWRS.2019.2894165

[29] Huang C, Wang C, Xie N, Wang Y. Robust coordination expansion planning for active distribution network in deregulated retail power market. IEEE Trans Smart Grid 2019;11(2):1476–88.

[30] Nourollahi R, Gholizadeh-Roshanagh R, Feizi-Aghakandi H, Zare K, Mohammadi-Ivatloo B. Power distribution expansion planning in the presence of wholesale multimarkets. IEEE Syst J 2022;17(1):1684–93.

[31] Lei Y, Wang D, Jia H, Chen J, Li J, Song Y, Li J. Multiobjective stochastic expansion planning based on multi-dimensional correlation scenario generation method for regional integrated energy system integrated renewable energy. Appl Energy 2020;276:115395. https://doi.org/10.1016/j.apenergy.2020.115395

[32] Kaisermayer V, Muschick D, Horn M, Gölles M. Progressive hedging for stochastic energy management systems. Energy Syst 2021;12:1–29. https://doi.org/10.1007/s12667-020-00401-z

[33] Kermani A, Cordeau J-F, Jans R. A progressive hedging-based matheuristic for the stochastic production routing problem with adaptive routing. Comput Oper Res 2024;169:106745.

[34] International Energy Agency. The future of heat pumps, Tech. rep. Paris: IEA; 2022. https://iea.blob.core.windows.net/assets/4713780d-c0ae-4686-8c9b-29e782452695/TheFutureofHeatPumps.pdf.

[35] Parlimant UK. Energy and Climate Change committee memorandum submitted by the Northern Ireland Executive; 2012.

[36] Pawlowicz R, Beardsley B, Lentz S. Classical tidal harmonic analysis including error estimates in Matlab using t-tide. Comput Geosci 2002;28(8):929–37.

[37] Aldersey-Williams J, Broadbent ID, Strachan PA. Analysis of United Kingdom offshore wind farm performance using public data: improving the evidence base for policymaking. Utilities Policy 2020;62:100985. https://doi.org/10.1016/j.jup.2019.100985

[38] Desalegn B, Gebeyehu D, Tamrat B, Tadiwose T, Lata A. Onshore versus offshore wind power trends and recent study practices in modeling of wind turbines' life-cycle impact assessments. Clean Eng Technol 2023;17:100691. https://doi.org/10.1016/j.clet.2023.100691. https://www.sciencedirect.com/science/article/pii/S2666790823000964.

[39] Pfenninger S. Dealing with multiple decades of hourly wind and PV time series in energy models: a comparison of methods to reduce time resolution and the planning implications of inter-annual variability. Appl Energy 2017;197:1–13. https://doi.org/10.1016/j.apenergy.2017.03.051

[40] Ahmad S, Abdullah M, Kanwal A, Tahir ZUR, Saeed U, Manzoor F, Atif M, Abbas S. Offshore wind resource assessment using reanalysis data. Wind Eng Aug. 2022. https://doi.org/10.1177/0309524X211069384

[41] Masihabadi D, Kalantar M, Majd Z, Saravi SVS. A novel information gap decision theory-based demand response scheduling for a smart residential community considering deep uncertainties. IET Gener Transm Distrib 2023;17(6):1383–99.

[42] Ji Z, Tian J, Liu S, Yang L, Dai Y, Banerjee A. Optimal scheduling of park-level integrated energy system considering multiple uncertainties: a comprehensive risk strategy-information gap decision theory method. Appl Energy 2025;377:124700. https://doi.org/10.1016/j.apenergy.2024.124700

[43] Sabzpoosh Saravi V, Kalantar M, Anvari-Moghaddam A. Resilience-constrained expansion planning of integrated power–gas–heat distribution networks. Appl Energy 2022;323:119315. https://doi.org/10.1016/j.apenergy.2022.119315.

[44] Sabzpoosh Saravi V, Kalantar M, Anvari-Moghaddam A. A cooperative resilience-oriented planning framework for integrated distribution energy systems and multi-carrier energy microgrids considering energy trading. Sustain Cities Soc 2024;100:105039. https://doi.org/10.1016/j.scs.2023.105039

[45] Zeng G, Liu M, Lei Z, Huang X. Bi-level robust planning of hydrogen energy system for integrated electricity–heat–hydrogen energy system considering multimode utilization of hydrogen. Energy 2024;303:132029. https://doi.org/10.1016/j.energy.2024.132029

[46] SONI. Soni publications and data archive; 2025. https://www.soni.ltd.uk/publications?page=1&pageSize=10&keyword=&sortBy=-created&categories=%7B%7D.

[47] Mier M, Azarova V. Investment cost specifications revisited. Energy Policy 2024;188:114058. https://doi.org/10.1016/j.enpol.2024.114058

[48] Krishnan S, Koning V, Theodorus de Groot M, de Groot A, Mendoza PG, Junginger M, Kramer GJ. Present and future cost of alkaline and PEM electrolyser stacks. Int J Hydrogen Energy 2023;48(83):32313–30. https://doi.org/10.1016/j.ijhydene.2023.05.031